



2D MXenes for Electromagnetic Shielding: A Review

Aamir Iqbal, Pradeep Sambyal, and Chong Min Koo*

Since the first report on electromagnetic interference (EMI) shielding of 2D $Ti_3C_2T_x$ in 2016, MXenes have captured the leadership position among lightweight shielding materials due to many advantages, including their excellent shielding performance, outstanding metallic conductivity, low density, large specific surface area, tunable surface chemistry, and solution processability. MXenes triggered a huge interest in the materials research community, leading to over 100 reported publications on MXenes' EMI shielding within 3 years. Many MXenes composites and hybrids in different structural forms, such as compact and laminate structures, layer-by-layer assemblies, porous foams and aerogels, and segregated structures, have been explored to further improve the intrinsic EMI shielding properties of MXenes. This article comprehensively reviews the recent advancements in MXene-based EMI shielding materials with different structural morphologies and provides an insight into future challenges and guidelines for finding material solutions for the next-generation shielding applications.

1. Introduction

The miniaturization of modern electronic devices and circuits has led to rapid growth in the technology and operating speeds of electronic systems. These miniaturized devices create undesirable electromagnetic interference (EMI) that can have detrimental effects on the performance of electronic systems.^[1–4] Prolonged exposure to electromagnetic (EM) radiation has a harmful effect on human health, causing nausea, headaches, eye problems,^[5] cancer,^[6] and adverse effects on infant brain development.^[7,8] Some medical implants or devices (e.g., hearing aids, insulin pumps, and cardiac pacemakers) are susceptible to malfunctions in an alternating EM field.^[9–13]

Modern warfare is also highly vulnerable to the effects of EMI, and the protection of forces and equipment against EM pollution or attack must be considered.^[14] Thus, the inhibition or mitigation of undesirable EM radiations has become an important field in materials science. Metals such as Cu, Al, Ag, and stainless steel have been widely used against EM pollution^[15–18] owing to their high conductivity. However, their high density, difficult processability, and high corrosion susceptibility have limited their applications in highly integrated modern mobile electronics. Various heterogeneous composites with conducting fillers such as 1D fillers (e.g., carbon nanofibers [CNFs] and carbon nanotubes [CNTs]), 2D fillers (e.g., expanded graphite, graphene, reduced graphene oxide, hBN, and MoS_2), magnetic fillers (Fe_3O_4 , Fe_2O_3 , and barium ferrite), and dielectric fillers (e.g., $BaTiO_3$, barium strontium titanate (BST), TiO_2 , and $PbTiO_3$) have been developed to replace metals for EMI shielding applications. These composites have advantageous properties, including lighter weight, better environmental stability, and excellent anticorrosive properties.^[19–23] However, their low shielding ability has limited widespread use.

2D MXenes are transition metal carbides, nitrides, and/or carbonitrides with the general formula $M_{n+1}X_nT_x$, where M is an early transition metal (e.g., Ti, Zr, V, Nb, Ta, or Mo), X is carbon and/or nitrogen, and T_x represents the functional groups on the surface of MXene.^[24] MXenes with additional surface terminal groups ($-OH$, $-O$, $-F$) can be produced to impart hydrophilicity via liquid state top-down synthesis in an acidic media that allows for easy processing and production of hybrids and composites in solution.^[25,26] MXenes possess all the fundamental characteristics required in an efficient EMI shielding material, namely good electrical conductivity, large specific surface area, light weight and, most importantly, ease of processability.^[1] Their tunable surface chemistry has facilitated the development of MXenes and composites with controlled structural designs such as compact laminates, layer-by-layer assemblies, porous and segregated structures. Following a breakthrough discovery in 2016 regarding the outstanding EMI shielding of 2D $Ti_3C_2T_x$,^[1] MXenes have become the leading lightweight EMI shielding material with the fastest growing number of related research publications (Figure 1).

This review highlights the effects of various MXene structural designs on the physical and electronic properties and EMI shielding mechanisms. The different structural approaches for MXenes in EM pollution inhibition are discussed comprehensively. Finally, the recent advances in MXenes-based EMI

A. Iqbal, Dr. P. Sambyal, Prof. C. M. Koo
 Materials Architecturing Research Center
 Korea Institute of Science and Technology
 Hwarangno 14-gil 5, Seongbuk-gu, Seoul 02792, Republic of Korea
 E-mail: koo@kist.re.kr

A. Iqbal, Prof. C. M. Koo
 Nanomaterials Science and Engineering
 University of Science and Technology
 217 Gajungro, 176 Gajung-dong, Yuseong-gu, Daejeon 34113, Republic of Korea

Prof. C. M. Koo
 KU-KIST Graduate School of Converging Science and Technology
 Korea University
 Anam-ro 145, Seongbuk-gu, Seoul 02841, Republic of Korea

The ORCID identification number(s) for the author(s) of this article can be found under <https://doi.org/10.1002/adfm.202000883>.

DOI: 10.1002/adfm.202000883

shielding materials and future research and development in the field are discussed in detail.

2. Mechanism of EMI Shielding

Various likely interaction mechanisms have been suggested for the interaction between incident EM radiation and both the surface and interior of a compact shield film with a defined single impedance or refractive index (**Figure 2a**). When an EM wave interacts with the shield, a portion of the incident power (P_I) is reflected (P_R) on the front and back surfaces due to an impedance mismatch between the shield and air. The remaining power is absorbed and dissipated as heat energy within the shield owing to attenuation or transmission (P_T).^[27]

The protection of a shield against the incident EM waves is defined as electromagnetic interference shielding effectiveness (EMI SE), which is expressed as a ratio of the transmitted and incident powers on a logarithmic scale, as shown in Equation (1).

$$SE_T \text{ (dB)} = 10 \log \frac{P_T}{P_I} = 20 \log \frac{E_T}{E_I} \quad (1)$$

where P and E represent power and electric field intensity, respectively, and subscripts I and T indicate incident and transmitted EM waves, respectively. The attenuation of EM radiation occurs via reflection, absorption, and multiple reflection mechanisms.^[28] Schelkunoffs theory^[29,30] states that the total EMI shielding effectiveness (EMI SE_T) is the sum of the attenuation achieved via reflection (SE_R), absorption (SE_A), and multiple reflection (SE_M), as is expressed in Equation (2).^[31–33]

$$SE_T = SE_R + SE_A + SE_M \quad (2)$$

2.1. Reflection Loss (SE_R)

Reflection is a primary EMI shielding mechanism caused by the interface or surface between the two propagation media (e.g., air and the shield) with different impedances or refractive indexes. The magnitude of reflection loss from the front to back of the shield surface can be quantified using a simplified version of Fresnel's equation for a highly conductive shield as follows:

$$SE_R \text{ (dB)} = 20 \log \frac{(\eta + \eta_0)^2}{4\eta\eta_0} = 39.5 + 10 \log \frac{\sigma}{2\pi f\mu} \quad (3)$$

where η and η_0 are the impedances of the shield and air, respectively, σ and μ are the electrical conductivity and the magnetic permeability of the shield, respectively, and f is the frequency of the incident EM waves. SE_R increases with increase in conductivity, indicating that the electrical conductivity of the shielding material must be high to achieve strong reflection loss. However, conductivity is not the only factor affecting reflection loss, and the permeability of the shield and frequency of EM waves also play a role.



Aamir Iqbal is currently a Ph.D. student at the Korea Institute of Science and Technology (KIST), under the University of Science and Technology (UST), Korea. His scientific interests are synthesis, characterization, and applications of advanced 2D materials for electromagnetic interference (EMI) shielding and bio-sensing applications.



Pradeep Sambyal received his Ph.D. in chemical sciences from the CSIR-National Physical Laboratory, India (2017). Currently, he is working as a postdoctoral researcher at KIST, Korea. His research focuses on nanomaterials for EMI shielding and anticorrosive coatings.



Chong Min Koo is currently center head and principal research scientist at the Materials Architecturing Research Center in KIST and also professor at the Korea University KU-KIST graduate school and the University of Science and Technology (UST). He received his M.S. (1999) and Ph.D. (2003) from the Korea Advanced Institute of Science and Technology (KAIST) in Daejeon, South Korea. He worked at the University of Minnesota (USA) as a postdoc (2005) and with LG Chemicals (2007) as a senior scientist. His research group is working on 2D MXenes, graphene, functional polymers, and nanocomposites for electromagnetic shielding and absorbing.

2.2. Absorption Loss (SE_A)

An EM wave is absorbed while propagating in a lossy medium (e.g., a shielding material) with an attenuation constant of α . The strength or amplitude (E) of the EM wave is exponentially diminished because $E = E_0 e^{-\alpha d}$ in a shield of thickness of d . The α value of the material can be expressed as a function of ω , μ , σ , and ϵ of the shield according to Equation (4).^[27,34]

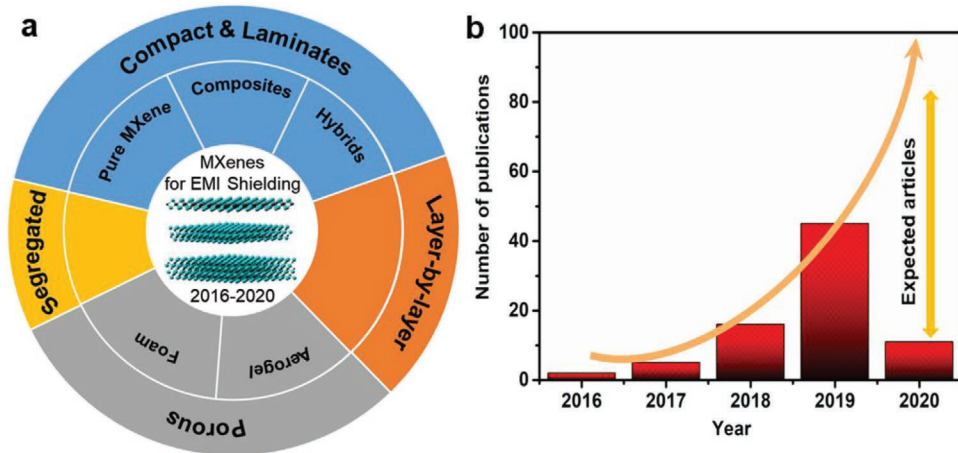


Figure 1. 2D MXenes serve as shields against EMI. a) The rise of different MXene structures for efficient EMI shielding and b) the number of publications focused on MXenes for EMI shielding (source: Scopus, 2020).

$$\alpha = \omega \sqrt{\frac{\mu\epsilon}{2}} \left[\sqrt{1 + \left(\frac{\sigma}{\omega\epsilon} \right)^2} - 1 \right] \quad (4)$$

where ω is angular frequency ($2\pi f$) and ϵ is dielectric permittivity. A high absorption loss requires the following conditions: high electrical conductivity for ohmic loss, which leads to increased interaction between the high electron density and the incident EM waves;^[1] large dielectric permittivity for dielectric loss, which is due to the formation of multiple micro- and

nano-capacitors;^[35] and large magnetic permeability for magnetic loss, which is associated with magnetic hysteresis loss and eddy current loss.^[36] Any absorbed energy shall dissipate in the form of heat energy.

The absorption loss (SE_A) for non-magnetic and conducting shielding materials is expressed as follows:

$$SE_A (\text{dB}) = 20 \log e^{\alpha d} = 20 \left(\frac{d}{\delta} \right) \log_{10} e = 8.68 \left(\frac{d}{\delta} \right) = 8.7 d \sqrt{\pi f \mu \sigma} \quad (5)$$

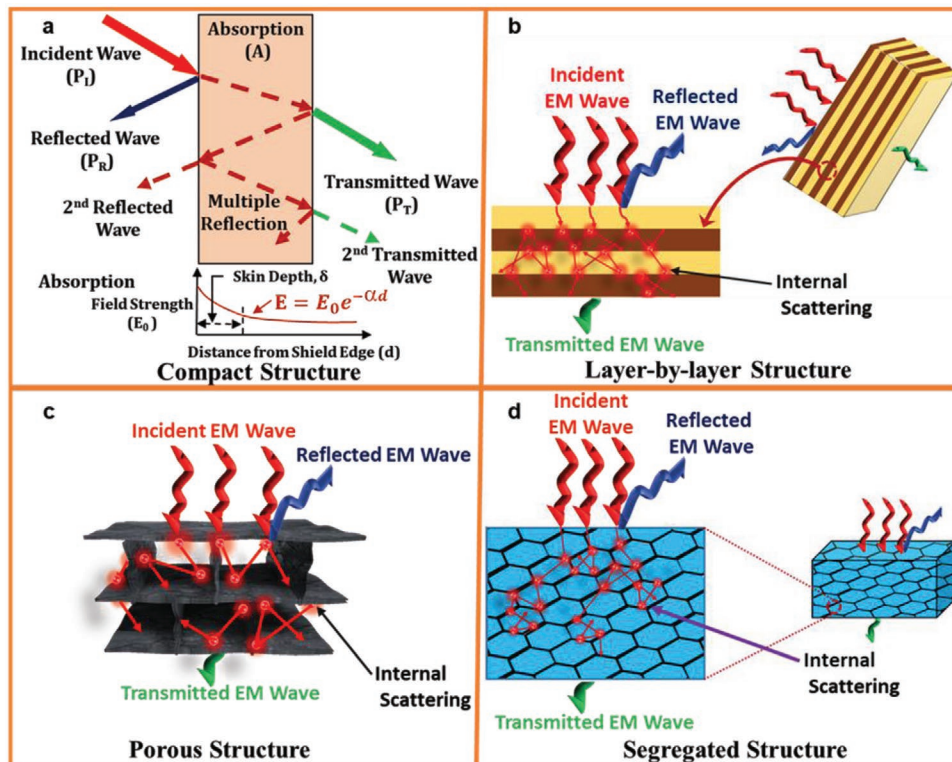


Figure 2. The interaction between incident electromagnetic waves and different structures, namely a) a compact film, b) layer-by-layer stacked morphology, c) porous structure, and d) segregated structure. Internal scattering occurs in the layer-by-layer, porous, and segregated structures only.

where δ is the skin or penetration depth. This is a useful term for shielding and represents the distance beneath the surface at which the intensity of the electric field decreases to $1 e^{-1}$ of the original incident wave intensity. For a conductive shield, the skin depth is expressed as $\delta = \frac{1}{\alpha} = (\sqrt{\pi f \mu})^{-1}$. The thickness and the electrical conductivity contribute majorly toward absorption, whereas permittivity and permeability determine absorption loss.

2.3. Multiple Reflections (SE_M)

In a thin shield, reflection from the back surface affects the final transmission owing to multiple reflection, as the reflected radiation re-reflects at the front surface and contributes to a second transmission. This can repeat until the energy of the wave is completely dissipated (Figure 2a). Multiple reflections between the front and back of the shield contribute a lower EMI SE. Multiple reflection (SE_M) is calculated as follows:

$$SE_M (\text{dB}) = 20 \log_{10} (1 - e^{-2\alpha d}) = 20 \log_{10} \left(1 - e^{-\frac{2d}{\delta}} \right) \quad (6)$$

SE_M is highly dependent on thickness and becomes negligible at a thickness close to or larger than the skin depth or when the SE_T reaches higher than 15 dB. However, if the thickness is much less than the skin depth, multiple reflection must be considered when investigating shield effectiveness.

2.4. Internal Scattering (Internal Multiple Reflections)

Shielding ability can be improved by introducing additional interfaces within the shield. Interfaces with mismatching impedance characteristics can contribute to additional internal scattering, also referred to as internal multiple reflections and consequently enhance absorption loss. The interactions between the shield and EM radiation in a layer-by-layer morphology (Figure 2b), porous structure (Figure 2c), and segregated structure (Figure 2d) have been illustrated with a schematic representation of the possible internal scattering shielding mechanisms. These structures provide additional interfaces that cause a large amount of internal scattering within the shield. Internal scattering extends the propagation path length of an EM wave before transmission and provides a higher chance of interaction between the shield and EM radiation, resulting in increased attenuation by absorption.^[37,38] Internal scattering should be distinguished from multiple reflection (SE_M) described in the previous section. Internal scattering caused by the extra internal interfaces inside the shield always contributes to increased absorption loss and total shielding effectiveness, while multiple reflection (SE_M) occurs between the front and back surfaces of the shield and lowers the shielding effectiveness.

2.5. Absolute Shielding Effectiveness

Light weight is a vital requirement in various applications, including aerospace and smart electronics. Absolute shielding

effectiveness (SSE/t) has been introduced to define the feasible shielding performance of a material while considering the density and thickness. SSE/t is calculated by dividing EMI SE by density (ρ) and thickness (t), where a high SSE/t is more desirable in lightweight shielding applications and is expressed in Equation (7) as^[1]

$$SSE/t = SSE_t = EMI SE / \rho / t = \text{dB cm}^2 \text{ g}^{-1} \quad (7)$$

3. MXenes as EMI Shielding Materials

3.1. MXene Compact Structures

3.1.1. MXene Laminates and Composites

Three different types of MXene laminate films have been reported, including single metal $Ti_3C_2T_x$, ordered double-metal $Mo_2TiC_2T_x$, and $Mo_2Ti_2C_3T_x$ MXenes.^[1] This previous study synthesized the MXenes from their corresponding MAX phases using a selective chemical etching protocol. Uniformly aligned MXene laminate films with few microns thickness were produced using vacuum-assisted filtration of their aqueous dispersions (Figure 3a,b). $Ti_3C_2T_x$ exhibited the largest EMI shielding efficiency owing to its superior electrical conductivity of $\approx 5000 \text{ S cm}^{-1}$, compared to 120 and 300 S cm^{-1} for $Mo_2TiC_2T_x$ and $Mo_2Ti_2C_3T_x$, respectively (Figure 3e). This study demonstrated that electrical conductivity is a crucial parameter in shielding (Figure 3f). The $Ti_3C_2T_x$ MXene exhibited an exceptional EMI SE of 48–92 dB in the X-band frequency range (8.2–12.4 GHz) while the average thickness increased from 1.5 to 45 μm (Figure 3g). The hydrophilicity of the $Ti_3C_2T_x$ MXene was advantageous and polymer composites with bio-compatible sodium alginate (SA) polymer were also prepared, where different mass ratios were investigated to optimize the mechanical and anti-oxidation properties (Figure 3c,d). A 90 wt% $Ti_3C_2T_x$ -SA composite film with a thickness of 9 μm exhibited an excellent EMI SE of 57 dB with the highest absolute shielding effectiveness (SSE/t) value exceeding $30000 \text{ dB cm}^2 \text{ g}^{-1}$. In comparison with the previously reported literature at the time, the $Ti_3C_2T_x$ MXene outperformed other conductive materials (i.e., graphite, graphene, CNFs, and CNTs) at the same thickness level and was comparable to metals (e.g., Ag and Cu) with electrical conductivities a few orders of magnitude greater (Figure 3i). It indicates that $Ti_3C_2T_x$ MXene is absolutely the best material for lightweight EMI shielding applications.

The excellent EMI SE of $Ti_3C_2T_x$ MXene films is attributed to an excellent electrical conductivity, as well as its laminate architecture due to the alignment of 2D flakes. When incident EM waves strike the surface of a highly conductive MXene, they are reflected because the numerous charge carriers (free electrons) in the MXene layers cause a high impedance mismatch at the MXene-air interface. The residual EM waves penetrate the MXene layered structure and are attenuated due to their strong interaction with high electron density MXene layers, where the mechanisms include eddy current and ohmic losses.

The excellent EMI shielding results of the $Ti_3C_2T_x$ MXene were supported by a later study,^[39] where theoretical calculations

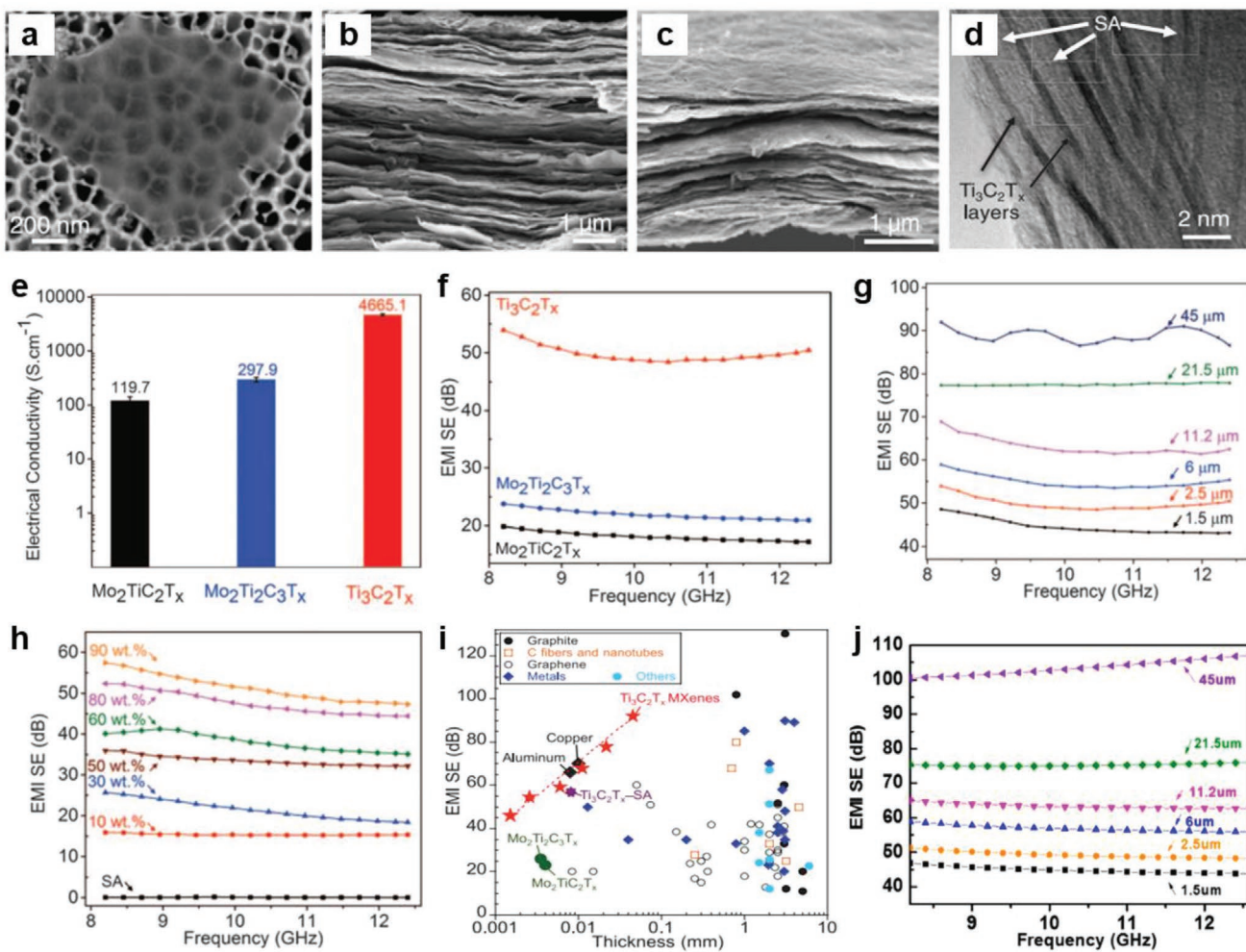


Figure 3. Scanning electron microscopy (SEM) images of a) exfoliated MXene flakes, and cross-sectional views of a bare MXene film (b) and MXene-SA composite film (c). d) Transmission electron microscopy (TEM) image of MXene-SA composite film. e) Electrical conductivity and f) EMI SE of $\text{Mo}_2\text{TiC}_2\text{T}_x$, $\text{Mo}_2\text{Ti}_2\text{C}_3\text{T}_x$, and $\text{Ti}_3\text{C}_2\text{T}_x$. g) EMI SE of $\text{Ti}_3\text{C}_2\text{T}_x$ MXene films of different thicknesses. h) EMI SE of 9 μm thick $\text{Ti}_3\text{C}_2\text{T}_x$ -SA composite films. i) EMI SE comparison of MXene films and their composites with other reported materials and j) validation of the findings by Shahzad et al.^[1] conducted by Li et al.^[39] a-i) Adapted with permission.^[1] Copyright 2016, American Association for the Advancement of Science (AAAS). j) Adapted with permission.^[39] Copyright 2018, MDPI.

were presented according to the Fresnel formula and attenuation rule. The theoretical calculations were consistent with the experimental results (Figure 3g,j), and emphasized the outstanding potential of $\text{Ti}_3\text{C}_2\text{T}_x$ MXene as a EMI shielding material.

A recent study investigated the shielding ability of nanometer-thick MXene laminate films and evaluated the effects of multiple reflections (SE_M).^[2] A large-area assembled monolayer MXene film was produced using interfacial self-assembly of MXene flakes (Figure 4a), while multilayered films were produced by repetitive stacking of the monolayer films (Figure 4b,c). The assembled monolayer $\text{Ti}_3\text{C}_2\text{T}_x$ MXene film with an average thickness of 2.3 nm exhibited excellent flexibility, transmittance above 90%, and sheet resistance of $1056 \Omega \text{ cm}^{-2}$. The absorbance increased and sheet resistance decreased with an increasing number of $\text{Ti}_3\text{C}_2\text{T}_x$ MXene layers (Figure 4d), while the EM shielding gradually increased (Figure 4e). While the monolayer $\text{Ti}_3\text{C}_2\text{T}_x$ MXene assembled film (2.3 nm) exhibited 1 dB EMI SE,

a 24 L MXene film with a thickness of 55 nm thickness offered 20 dB and a 99% shielding efficiency (Figure 4f). A maximum absolute shielding effectiveness of $3.89 \times 10^6 \text{ dB cm}^2 \text{ g}^{-1}$ was obtained from an annealed film.

A systematic evaluation of shielding mechanisms has been conducted, where two different models were considered, namely Simon's formula^[40] and the transfer matrix method.^[41-43] Simon's formula only accounts for reflection (SE_R) and absorption (SE_A), while the transfer matrix method considers all possible shielding mechanisms, including multiple reflections (SE_{MR}), SE_R , and SE_A .

A study of micrometer-thick MXene films found a linear increase in SE_T at a thickness above 1.5 μm , as predicted by Simon's formula (Figure 4g-i).^[1] However, Simon's formula could not predict the experimental results at a thickness less than the skin depth (7.86 μm for $\text{Ti}_3\text{C}_2\text{T}_x$), highlighting the substantial effects of multiple reflection in thinner films. The reflected waves underwent repeated reflections and absorptions

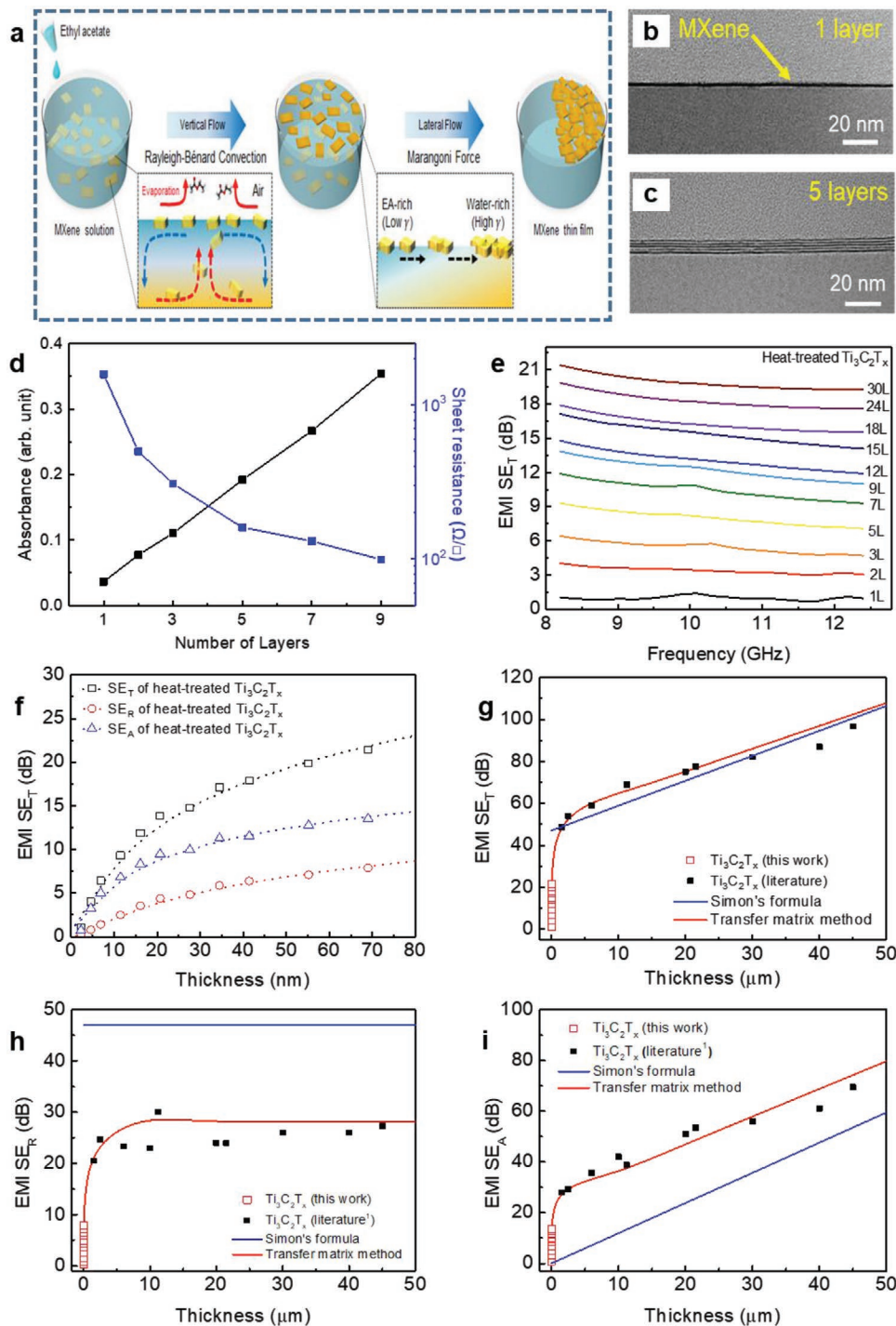


Figure 4. a) Fabrication of an interfacially self-assembled MXene thin film; cross-sectional images of b) monolayer (1L) and c) 5-layer (5L) films. d) Sheet resistance and optical absorbance at 550 nm for MXene films with varying numbers of layers. e) EMI SE_T in the X-band frequency range for annealed (400 °C) MXene films with varying numbers of layers. f) The EMI SE_T , SE_R , and SE_A values of electrically thin MXene films measured experimentally and calculated using the transfer matrix method. The g) EMI SE_T , h) SE_R , and i) SE_A values calculated using the transfer matrix method (red line) and Simon's formula (blue line), and measured experimentally in the current study (red dots) and in a study by Shahzad et al.^[1] (black dots). Adapted with permission.^[2] Copyright 2020, Wiley-VCH.

within the shielding material until the wave is either transmitted or completely attenuated (Figure 2a), resulting in a lower SE_T , higher SE_A , and lower SE_R contributions.

A customized architecture can be achieved within MXene laminates using vacuum filtration or interfacial assembly of 2D flakes and can increase the attenuation of incident EM

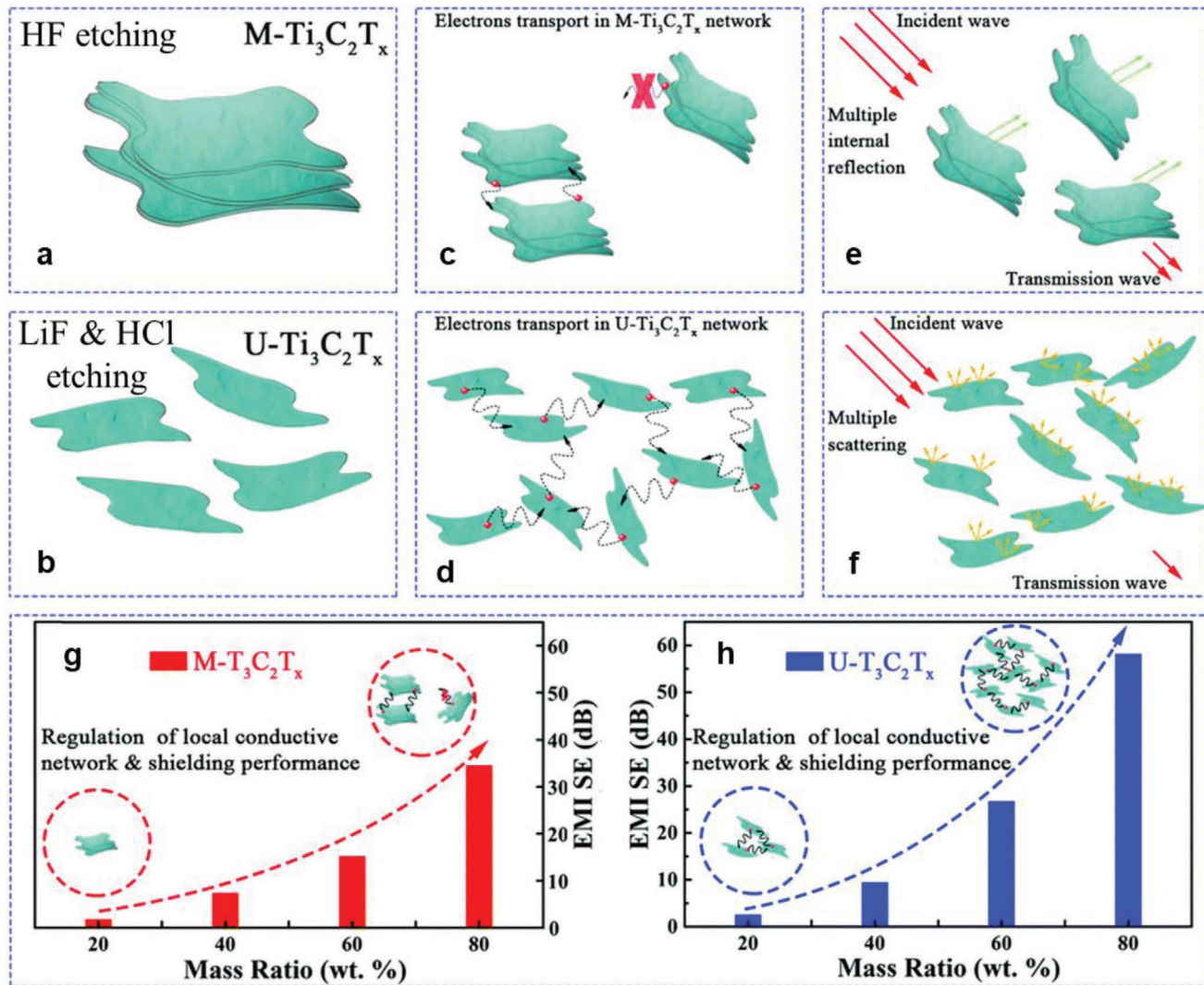


Figure 5. Structural morphology and proposed EM interaction within M-Ti₃C₂T_x and U-Ti₃C₂T_x composites. The microstructure of a) M-Ti₃C₂T_x and b) U-Ti₃C₂T_x. The local conductive network of c) M-Ti₃C₂T_x and d) U-Ti₃C₂T_x. The microwave propagation model in e) M-Ti₃C₂T_x and f) U-Ti₃C₂T_x, and the regulation of local conductive network and shielding performance for g) M-Ti₃C₂T_x and h) U-Ti₃C₂T_x. Reproduced with permission.^[44] Copyright 2019, The Royal Society of Chemistry.

waves within the structure. Electrically thin MXene laminate films (thickness = nanometers) exhibit the same absorption dominant shielding mechanism ($SE_A > SE_R$) as electrically thick films (micrometers). Electrically thin films are susceptible to a high incidence of multiple reflections, and the efficient shielding performance at a nanometer thickness shows promise for shielding of unwanted EM waves in advanced, highly integrated, and lightweight smart electronic devices.

The EMI shielding capabilities of Ti₃C₂T_x MXene synthesized by two different routes were evaluated (as shown in Figure 5).^[44] Both protocols involved the etching of Ti₃AlC₂ MAX powder, where the first used 40% hydrofluoric acid (HF) at room temperature for 24 h to obtain an accordion-like multilayered (M-Ti₃C₂T_x) morphology, and the second used LiF and HCl for 16 h at 40 °C to obtain delaminated ultrathin (U-Ti₃C₂T_x) MXene sheets. The M-Ti₃C₂T_x composite possessed more –F terminations, while the U-Ti₃C₂T_x composite was rich

in =O terminations. Both Ti₃C₂T_x MXenes were mixed with an EM transparent matrix of SiO₂ nanoparticles in different mass ratios (20, 40, 60, and 80 wt%) and cold pressed under 5 MPa. The U-Ti₃C₂T_x composite exhibited superior electrical conductivity (4.2×10^{-3} S cm⁻¹) at 60 wt% MXenes compared to M-Ti₃C₂T_x (6.3×10^{-5} S cm⁻¹). An EMI SE of 58 dB was achieved from the 1 mm thick 80 wt% U-Ti₃C₂T_x MXene composite in the frequency range of 8.2–12.4 GHz. The U-Ti₃C₂T_x MXene composites exhibited superior EMI shielding capabilities than M-Ti₃C₂T_x due to a higher electrical conductivity, larger surface area, and more conductive networks. Furthermore, the larger exposed surface area of the U-Ti₃C₂T_x MXene composite contained a large number of surface terminations and point defects, which resulted in increased dipolar polarization loss and more attenuation.

Li et al. studied a Ti₂CT_x MXene produced using chemical etching of a Ti₂AlC MAX phase using a slightly modified LiF

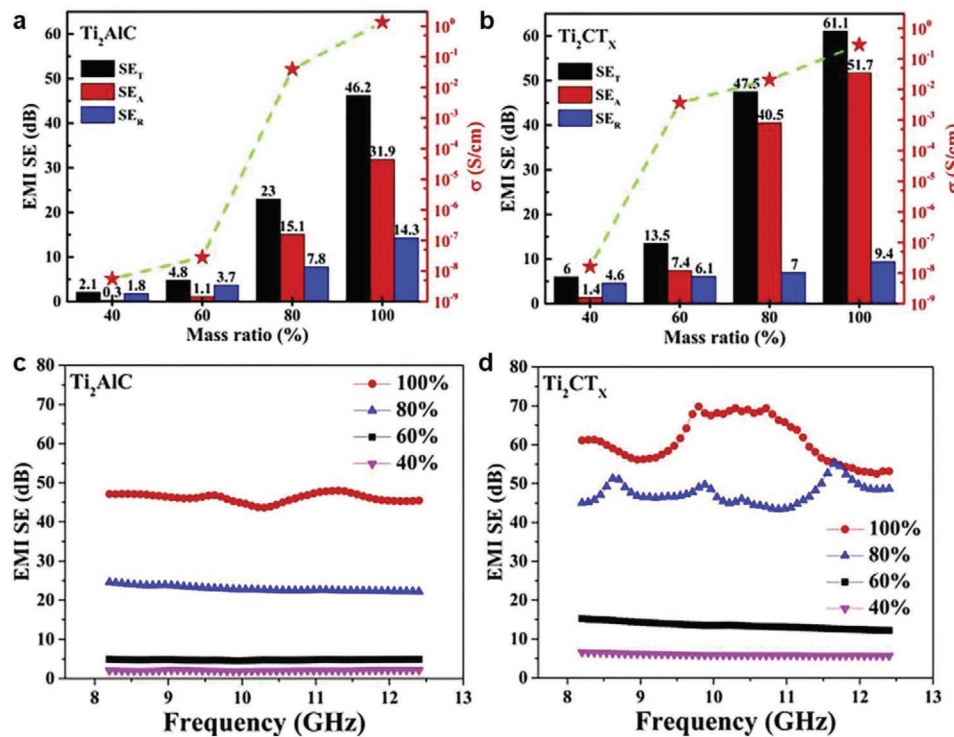


Figure 6. The electrical conductivity and average EMI SE values of a) Ti₂AlC MAX and b) Ti₂CT_x MXene in a wax matrix at various mass ratios; and the detailed SE_T curves of c) Ti₂AlC MAX and d) Ti₂CT_x MXene in a wax matrix at various mass ratios in the X-band frequency range (8.2–12.4 GHz). Adapted with permission.^[45] Copyright 2019, Elsevier.

and HCl method.^[45] Ti₂AlC and the laminar Ti₂CT_x MXene were mixed in a paraffin wax matrix in mass ratios ranging from 40 to 100 wt%, and the electrical conductivity and EMI shielding performances in the X-band frequency range of the resulting composites were evaluated. Despite the lower electrical conductivity (0.30 S cm^{-1}) of the Ti₂CT_x MXene in comparison with the pure Ti₂AlC MAX (1.37 S cm^{-1}), the electrical conductivity values of the Ti₂CT_x MXene-based composites were larger than that of Ti₂AlC MAX-based composites at 40 wt%, where the values for Ti₂CT_x/paraffin composite and Ti₂AlC/paraffin composites were 1.63×10^{-8} and $5.57 \times 10^{-9}\text{ S cm}^{-1}$, respectively. The exfoliated Ti₂CT_x MXene sheets had a larger surface area that allowed for the efficient construction of a strong conductive network, even at comparatively lower mass ratios. The superior electrical conductivity of the delaminated Ti₂CT_x MXene led to a higher EMI SE of 70 dB, while the EMI SE of the Ti₂AlC MAX phase was 46.2 dB at thickness >0.8 mm (Figure 6a–d).

Laminates of Ti₃C₂T_x MXenes owe their superior EMI shielding effectiveness to an excellent electrical conductivity of 5000 to 10 000 S cm⁻¹.^[46] However, a smaller flake size of 2D MXene sheets can lead to weaker mechanical properties and poor resistance against oxidation in practical applications. Thus, the development of strong and tough MXenes' hybrids and composites has grown in popularity. The homogenous dispersion of 1D nanofibers, nanowires, or polymeric chains into 2D MXene nanosheets synergistically imparts composite films with mechanical strength and improves the EMI shielding efficiency. Nanofibers and nanowires can act as stress-distributors under tension, while polymers produce a brick-and-mortar type

structure to give a flexible, tough, and mechanically strong structure. Reinforcement with nanofibers, nanowires, and polymeric chains also introduces hydrophobicity to improve the oxidation resistance of the composites.^[47–49]

Ti₃C₂T_x-cellulose nanofiber (MXene-CNF) composites with nacre-like structure have been produced using a simple vacuum-assisted filtration method, and the EMI shielding and mechanical properties of the composites were evaluated (Figure 7a).^[47] The distribution of 1D nanofibers resulted in less insulated contacts between the 2D MXene nanosheets, which retained the high electrical conductivity that increased further with increase in the MXene content (Figure 7b). A 47 μm thick nanocomposite with 80 wt% Ti₃C₂T_x had an electrical conductivity of 1.155 S cm^{-1} and EMI SE of 25.8 dB at 12.4 GHz. The addition of tough nanofibers improved the mechanical properties of the composite films, which were found to be superior to pure MXene and even pure CNF paper. An ultimate tensile strength of 135.4 MPa and fracture at strain of 16.7% was obtained at 50 wt% Ti₃C₂T_x. This strength was attributed to the mother of pearl type structure of the composite film formed due to strong hydrogen bonding between the hydroxyl groups on the CNF and MXene surfaces. Hydrogen bonding allowed the composite to endure more stress under tension by maintaining the well-stacked and compact morphology even after fracture. For these reasons, flexible MXene composites are popular candidates for foldable and wearable electronics.

A recent study investigated the mechanical properties of ultrathin MXene-aramid nanofiber (ANF, commonly known as Kevlar) composite for EMI shielding.^[50] A lower MXene content

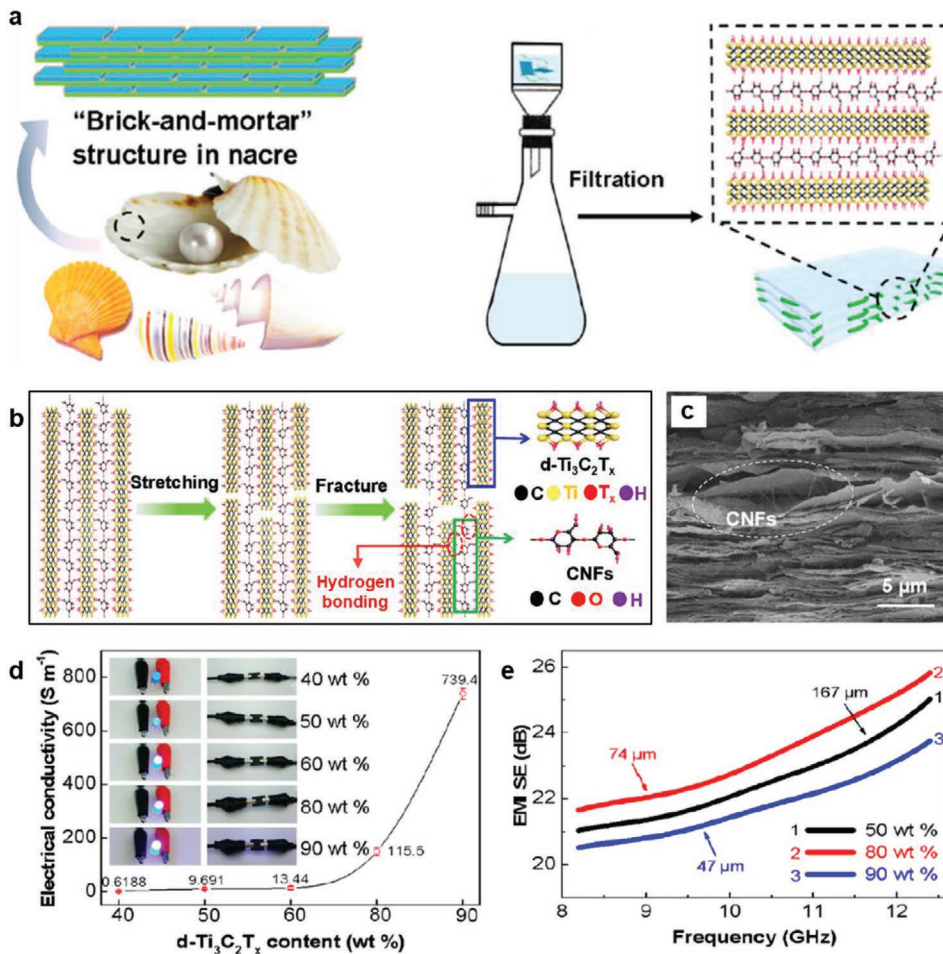


Figure 7. a) The brick-and-mortar structure of mother of pearl. The b) fracture mechanism and c) SEM image of the fractured surface of d-Ti₃C₂T_x/CNF composite paper. d) The electrical conductivity of d-Ti₃C₂T_x/CNF composite paper sheets with varying d-Ti₃C₂T_x contents. e) The EMI SE of d-Ti₃C₂T_x/CNF composite paper sheets with varying d-Ti₃C₂T_x contents and thicknesses. Adapted with permission.^[47] Copyright 2018, American Chemical Society.

(<10 wt%) improved the mechanical properties of pure ANF paper and reached a maximum of 197 MPa and 9.8% for ultimate tensile strength and the fracture strain, respectively. Further addition of MXene increased the electrical conductivity and EMI SE of a 17 μm thick film to 170 S cm⁻¹ and 33 dB, respectively.

Non-conducting polymers are useful in the development of MXene composites with good mechanical properties. The EMI shielding of vacuum filtered Ti₃C₂T_x/hydroxyethyl cellulose (MXene/HEC) nanocomposite were studied,^[49] where confined organic chains of HEC improved the mechanical strength of the composite by forming hydrogen bonds with MXene's hydroxyl terminations (—OH groups). A 100 μm thick MXene/HEC composite exhibited an EMI SE of 24 dB in the measured X-band frequency range.

Low-temperature annealed (200 °C for 2 h) Ti₃C₂T_x MXene/epoxy composites have been produced using a solution casting method.^[51] The electrical conductivity of the insulating epoxy (2.2×10^{-12} S cm⁻¹) was adjusted to 0.38 S cm⁻¹ for the unannealed and 1.05 S cm⁻¹ for the annealed 15 wt% Ti₃C₂T_x/epoxy composites, with EMI SE of 30 dB and 41 dB, respectively at 2 mm thickness.

Conducting polymers help in retaining good electrical conductivity in MXene-based composites. Conductive chains in between MXene layers create a conductive path to aid the flow of electrons. Vacuum filtered Ti₃C₂T_x MXene and PEDOT:PSS nanocomposites have been developed for EMI shielding applications.^[52] The brick-and-mortar structure of the mother of pearl type composite included 2D MXene sheets within the framework to act as bricks and conductive organic polymer chains as mortar and resulted in a high electrical conductivity (Figure 8a,c). The conductivity of pure Ti₃C₂T_x is 1000 S cm⁻¹ and was lowered to 340.5 S cm⁻¹ in the composite with a Ti₃C₂T_x to PEDOT:PSS ratio of 7:1, whereas the EMI shielding efficiency of both materials was ≈42 dB at a thickness of 11.1 μm (Figure 8b) and the density of the composite was much lower at 1.94 g cm⁻³. The structure of the composite maintained the electrical characteristics of pure MXene. Incident EM radiation was able to enter the structure and the waves were attenuated via various polarization mechanisms at the interfaces between the highly conducting MXene sheets and the less conductive PEDOT:PSS.

Vacuum filtered ultrathin Ti₃C₂T_x/polyaniline (MXene-PANI) composites were also investigated for EMI shielding.^[53]

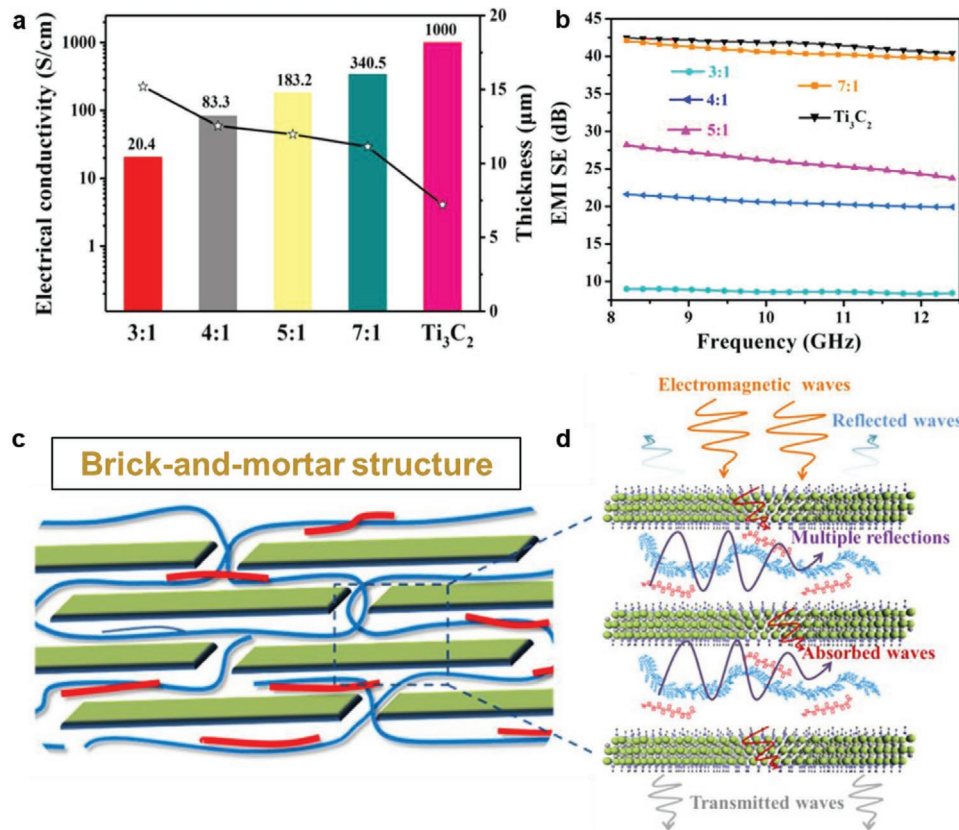


Figure 8. The a) electrical conductivity and thickness, and b) EMI SE of the pure Ti₃C₂T_x MXene and polymeric composite films with different ratios. The c) brick-and-mortar structure and d) EMI shielding mechanism of the film. Adapted with permission.^[52] Copyright 2018, American Chemical Society.

Conductive polymeric chains between the MXene layers improved the electrical conductivity (24.4 S cm^{-1}), giving a EMI SE of 36 dB at 40 μm thickness.

3.1.2. MXene Hybrids

MXene hybrids incorporate other conducting or magnetic ingredients to further enhance the shielding effectiveness. Multiple phases synergistically enhance the interaction between incident EM waves and the structure, and can improve mechanical properties. Ultrathin and lightweight TiO₂-Ti₃C₂T_x/graphene hybrid laminate films have been developed for EMI shielding applications.^[54] A very thin (5–9 μm) Ti₃C₂T_x/graphene oxide film was produced using vacuum filtration, followed by thermal treatment at 1000 °C in an inert argon atmosphere to oxidize the MXene sheets (as Ti₃C₂T_x is stable in inert atmosphere up to 800 °C) and produce TiO₂-Ti₃C₂T_x/graphene hybrid films. Hybrid laminate films with varying MXene contents were prepared to investigate the role of dielectric TiO₂ particles in highly conductive MXene laminates. The high surface resistance of the pure graphene films was gradually decreased ($75 \Omega \text{ cm}^{-2}$) with the addition of highly conductive MXenes. The improved electrical conductivity of the hybrid film contributed to a good EMI shielding efficiency of 28 dB at a thickness of 9.17 μm . The TiO₂ particles allowed for the formation of miniature capacitor-like structures that dissipated

the EM energy via a dipolar polarization mechanism and dielectric losses.

Flexible, lightweight, and hydrophobic MXene and graphene-based hybrids in PVDF were produced using cost-effective spray coating and solvent casting methods.^[55] The 0.35 mm thick MXene-graphene-PVDF hybrid had an electrical conductivity of 13.68 S cm^{-1} , an EMI SE of 41 dB in the S-band and 54 dB in the X-band, and improved thermal stability. These MXene-graphene-PVDF composites can be used in humid and hot environments where other materials tend to fail or degrade under ambient conditions.

The synergistic effect of conductive CNTs and CNFs for EMI shielding and mechanical properties in Ti₃C₂T_x MXenes has been investigated.^[48] The tensile strength of the hybrid film was 97.9 MPa, while the fracture strain was 4.6%. A 38 μm thick CNT/MXene/CNF hybrid film exhibited an electrical conductivity and EMI SE of 25.06 S cm^{-1} and 38.4 dB, respectively, which is much higher than a MXene/CNF nanocomposite with comparable thickness.

Dielectric and magnetic losses can occur in efficient EMI shielding materials across a wide frequency range. MXene/Ni chain hybrids with PVDF have been produced for efficient EMI shielding using a simple solution casting method.^[56] The PVDF/MXene/Ni chain hybrid included 2D MXene sheets and 1D Ni chains that were in close contact. The electron conduction was improved, where the electrical conductivity of the P-10M10N hybrid (10 wt% of MXene and 10 wt% Ni chains)

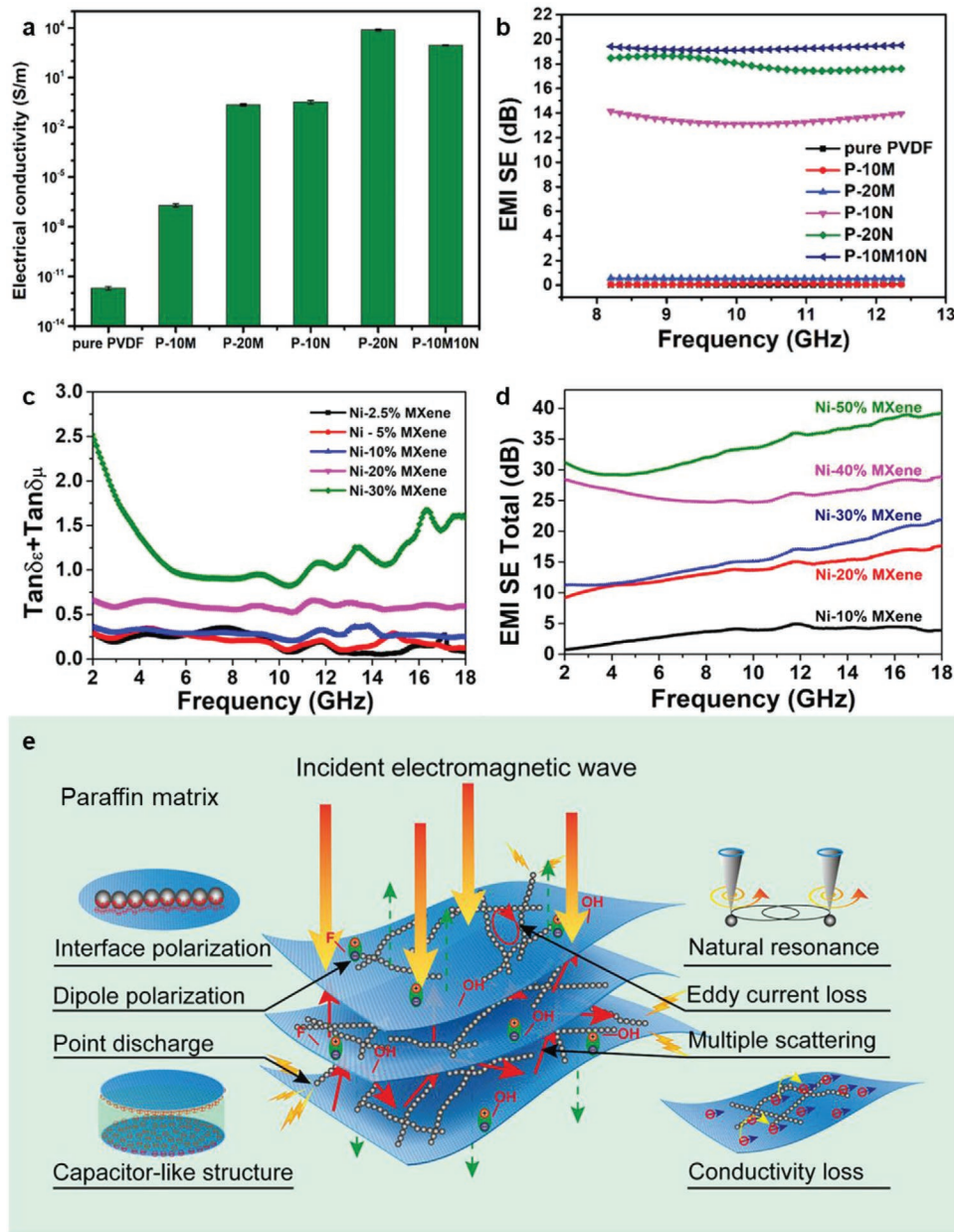


Figure 9. The a) electrical conductivity and b) EMI SE of PVDF/MXene/Ni chain composite films with varying compositions. c) The frequency dependence of $\tan \delta_e + \tan \delta_\mu$ and d) EMI SE of MXene/Ni hybrid composites in wax with varying MXene contents. e) The EM radiation loss mechanisms in the MXene/Ni hybrid. a,b) Adapted with permission.^[56] Copyright 2019, Wiley-VCH. c–e) Adapted with permission.^[57] Copyright 2019, American Chemical Society.

reached a maximum of $\approx 8.92 \text{ S cm}^{-1}$ (Figure 9a). A P-10M10N film of 0.1 mm thickness exhibited an EMI SE value of 20 dB (Figure 9b) that further increased to 35 dB at 0.36 mm. A similar study evaluated $\text{Ti}_3\text{C}_2\text{T}_x$ MXene/Ni nano-chain hybrids with varying MXene contents in a wax matrix.^[57] The MXene/Ni chain hybrids were produced using a low-temperature hydrothermal process (60°C for 4 h). The Ni chains had an average length of $20 \mu\text{m}$ and consisted of interconnected Ni nanoparticles with diameters of $\approx 300 \text{ nm}$. At a fixed Ni content of 10 wt%, ring-shaped paraffin-based composites (inner diameter = 3.04 mm, outer diameter = 700 mm) with varying

MXene contents were prepared. At 50 wt% MXene content (above percolation threshold), the highly conductive MXenes dramatically increased the electrical conductivity of the insulating PVDF from 7.1×10^{-14} to 0.04 S cm^{-1} . The sum of dielectric loss tangent ($\tan \delta_e$) and magnetic loss tangent ($\tan \delta_\mu$) positively increased with the addition of MXenes and Ni chains (Figure 9c), thus enhancing the absorption of EM radiation. The uniform coating of MXene sheets with Ni chains produced multiple interfaces that contributed toward substantial interfacial polarization under an applied EM field. A maximum EMI SE value in the range of 34 to 40 dB was achieved in the

1.3 mm thick 50 wt% of MXene hybrid (Figure 9d). The excellent electrical conductivity of the hybrid resulted in conduction losses within the system, and the EM radiation was attenuated via electron migration and electron hopping (Figure 9e). The dipole polarization attributed to the surface terminations of the MXene and the intrinsic magnetic properties of Ni chains both contributed toward magnetic losses and the absorption of EM radiation. Thus, MXenes and magnetic Ni chains work synergistically to achieve excellent EMI shielding behavior in a hybrid composite.

3.2. Layer-by-Layer Structured MXenes

Layer-by-layer (LbL) assembly of two phases with different impedances can cause major internal scattering at the internal interfaces and aids the attenuation of the incident EM radiation. LbL structures can be produced using various solution-processing techniques, including spin coating,^[58] spray coating,^[59] dip coating,^[60] solution casting,^[61] and interfacial assembly.^[62] Stable dispersions of exfoliated MXene sheets in aqueous and organic solvents can be prepared due to their surface hydrophilicity, which allows for processing with a number of nanostructures and polymers using solution-processing methods.^[63] An LbL structure using two distinct alternating layers can also improve the mechanical strength.

Semi-transparent films have been recently produced from the alternate layer-by-layer (LbL) deposition of $Ti_3C_2T_x$ -polyvinyl alcohol (PVA) and single/multi-wall CNT-poly sodium 4-styrene sulfonate (CNT-PSS) dispersions using spin-spray coating on a rotating glass substrate (Figure 10a).^[64] The thickness and uniformity of the films were systematically controlled by the amount of dispersion and the rotational speed of the substrate, as well as the number of $Ti_3C_2T_x$ -CNT bilayers. The compacted composite films exhibited good transparency that linearly decreased with an increasing number of bilayers. A 300 bilayer film with a thickness of ≈ 200 nm had an electrical conductivity of $130 S cm^{-1}$, attributed to the highly conductive $Ti_3C_2T_x$ MXene and CNTs, and an EMI SE and absolute EMI SE (SSE/t) of 2.9 dB and $58.187 dB cm^2 g^{-1}$, respectively.

Dual functional MXene/PVA composites have been produced using the LbL assembly of $Ti_3C_2T_x$ MXene and polyvinyl alcohol (PVA) via a simple liquid casting method.^[65] The first layer of aqueous PVA solution was cast on a clean iron substrate and completely dried at $45^\circ C$. MXene layer of varying concentrations was deposited on the PVA layer and dried under the same conditions. This process was repeated until a predetermined thickness with a final top layer of PVA (Figure 11a). The composites with varying $Ti_3C_2T_x$ MXene contents (7.5, 13.9, and 19.5 wt. %) were produced using a different number of stacking cycles. The multilayered compacted films

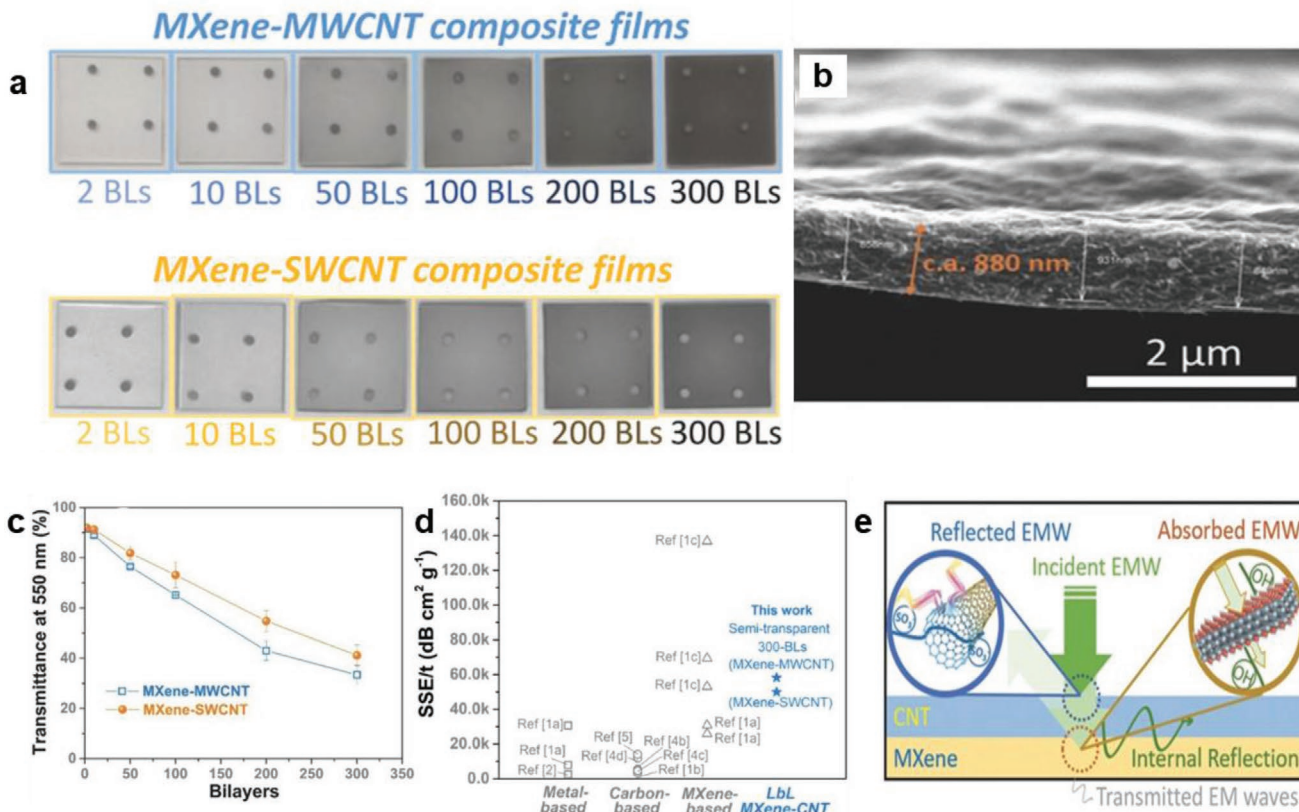


Figure 10. a) The LbL assembly of a $Ti_3C_2T_x$ -CNT composite film; b) MXene-SWCNT composite films with various numbers of bilayers; c) the transmittance and conductivity of MXene-MWCNT and MXene-SWCNT composite films; d) a comparison of specific EMI SE (SSE/t) in various materials; and e) the proposed EMI shielding mechanism of a multilayered MXene-CNT composite film. Adapted with permission.^[64] Copyright 2018, Wiley-VCH.

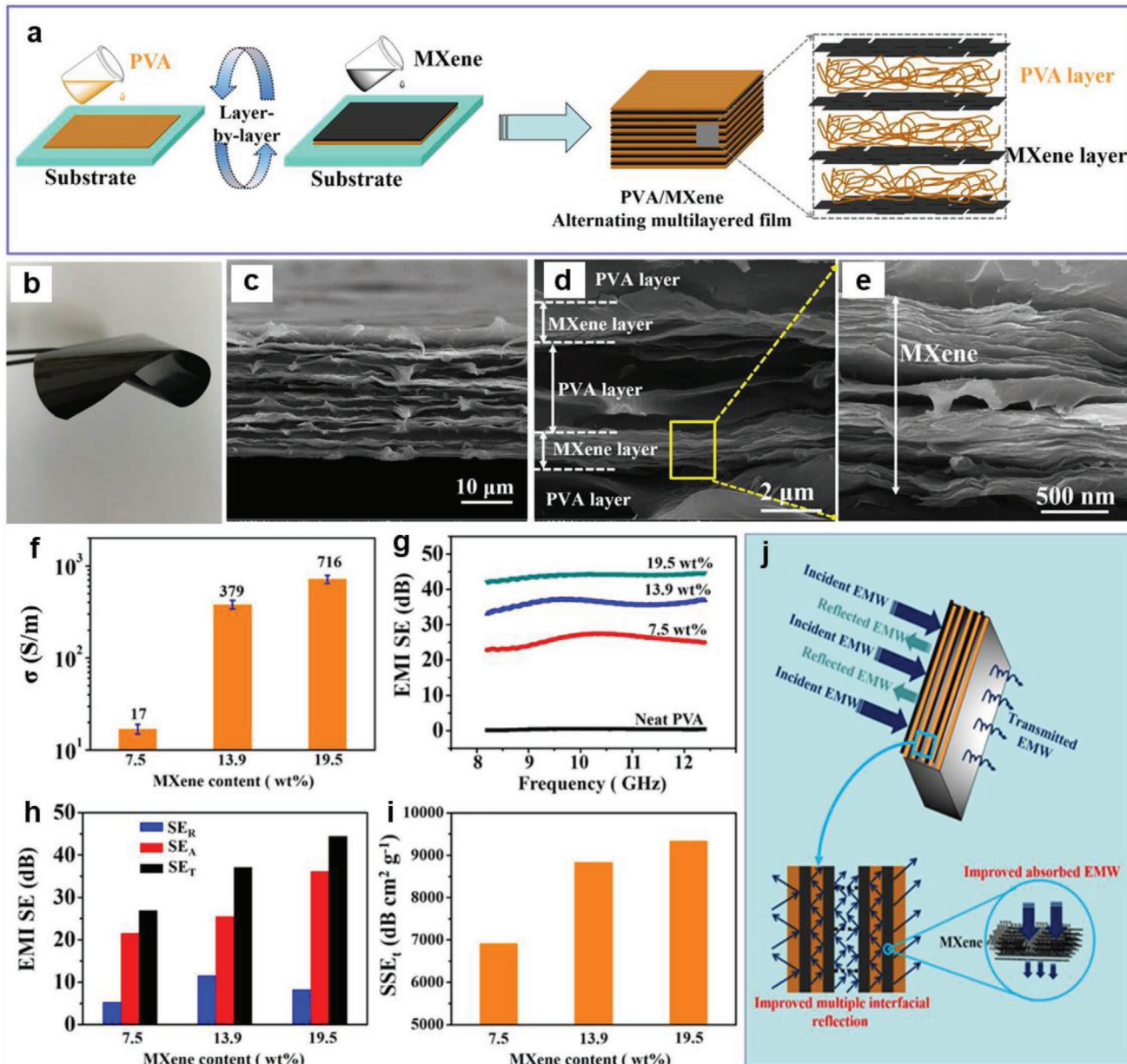


Figure 11. a) The fabrication of MXene/PVA multilayered composite films via multilayered casting; b) digital image of the flexible MXene/PVA-AM-19.5 film; c–e) SEM images of MXene/PVA-AM-19.5 film at different magnifications; f) the electrical conductivity of various PVA/MXene multilayered films; g) the EMI SE of pure PVA and various PVA/MXene multilayered films in the X-band frequency range; h) a comparison of the SET, SEA, and SER of various PVA/MXene multilayered films at 10 GHz; i) the specific SE (SSE_t) of various PVA/MXene multilayered films; and j) EM wave dissipation in the PVA/MXene multilayered films. Adapted with permission.^[65] Copyright 2019, Elsevier.

exhibited excellent mechanical flexibility due to the use of PVA in conjunction with $\text{Ti}_3\text{C}_2\text{T}_x$ MXene, where each layer was 1 to 3 μm thick. The composite films exhibited an electrical conductivity up to 7.16 S cm^{-1} that improved with increase in $\text{Ti}_3\text{C}_2\text{T}_x$ MXene content (Figure 11f). The EMI shielding followed a similar trend and reached a maximum of 44.4 dB for the highest $\text{Ti}_3\text{C}_2\text{T}_x$ MXene content at a thickness of 25 μm (Figure 11g). The multilayered stacked LbL geometry with alternating conducting and non-conducting layers had mismatched impedance and enhanced the internal scattering and absorption of EM radiation.

$\text{Ti}_3\text{C}_2\text{T}_x$ MXene and silver nanowire (AgNW) decorated silk fabrics ($\text{MA}_x)_n$ were produced using vacuum-assisted LbL spray coating, where M is MXene, A is AgNW, x is AgNW concentration, and n is the number of spraying cycles.^[66] $\text{Ti}_3\text{C}_2\text{T}_x$ and AgNW dispersions were alternatively sprayed on the silk fabric using atomizers and repeated for both sides of the substrate. The composite exhibited a leaf-like nanostructure with $\text{Ti}_3\text{C}_2\text{T}_x$ as the conductive lamina and AgNWs as the conductive veins (Figure 12b–d). The sheet resistance decreased linearly with increase in AgNW concentration (n). However, a higher concentration resulted in a continuous film on the substrate that

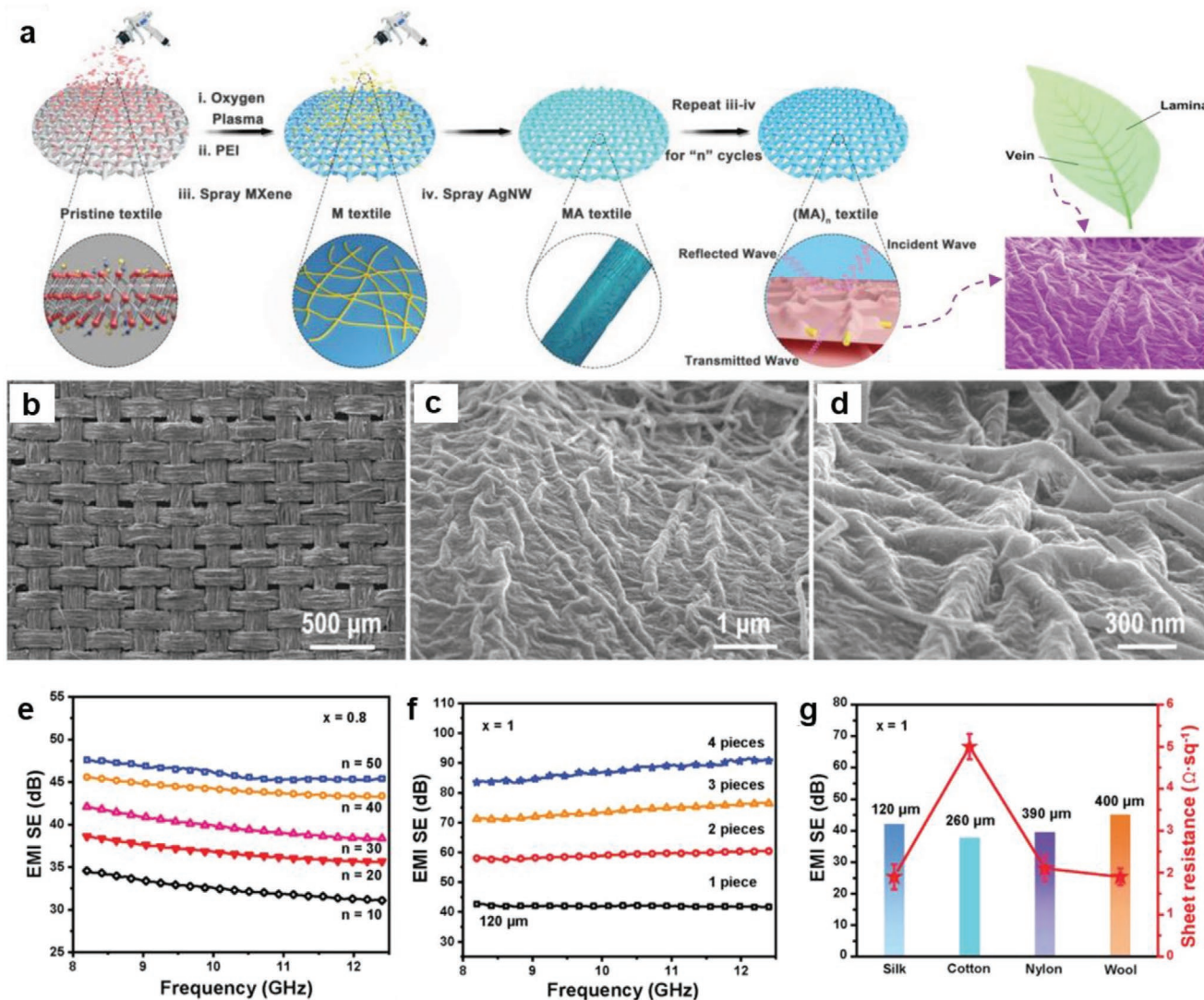


Figure 12. a) The fabrication of hydrophobic, permeable and conductive silk textiles using vacuum-assisted layer-by-layer assembly; b-d) (MA)₂₀ silk under various magnifications; e) the EMI SE of (MA_{0.8})_n silk textiles produced using various numbers of spray cycles; f) the EMI shielding performance of (MA₁)₁₀ silk textile with varying thicknesses; and g) the EMI shielding performance and sheet resistance of (MA₁)₁₀ textiles with various textile substrates (silk, cotton, nylon, and wool). Adapted with permission.^[66] Copyright 2019, Wiley-VCH.

reduced the air permeability of the composite. Air permeability of the composite was analyzed for flexible electrode and EMI shielding measurements. EMI shielding efficiency increased linearly with an increasing number of cycles and AgNWs content (Figure 12e). The leaf-like structure was 120 μm thick and resulted in an EMI SE of 54 dB in the X-band frequency range (Figure 12f).

Flexible and wearable textiles have been coated with $Ti_3C_2T_x$ MXene/polypyrrole (PPy) for EMI shielding applications.^[67] A polyethylene terephthalate (PET) fabric was repeatedly dipped into a dispersion of MXene sheets modified with in situ polymerized PPy chains. The fabric was subsequently coated with silicon for textile hydrophobicity. The electrical conductivity of the non-conductive PET fabric increased linearly with increase in $Ti_3C_2T_x$ MXene content and concentration, and was ≈ 10 S cm⁻¹ after ten cycles. The improved electrical

conductivity led to outstanding EMI shielding of 42 dB while maintaining the air permeability of the fabric. The EMI SE was further increased by increasing the number of cycles or combining numerous pieces of the MXene/PPy coated fabric. A maximum value of 90 dB was achieved by laminating three 0.45 mm thick pieces. The additional top silicon coating rarely affects the electrical conductivity and EMI shielding properties of a coated fabric but is effective in maintaining hydrophobicity of the membranes for long-term and multi-wash usage. The hydrophilicity of 2D MXene sheets can be used to produce customized properties and may be paired with an additional hydrophobic coating layer if required for the final application.

$Ti_3C_2T_x$ MXene/tandem repeat protein (TR42)-based ink has been printed on a flexible PET substrate while heated to 70 °C.^[68] Continuous printing with a resolution (minimum width of printed line) of 120 μm was achieved using

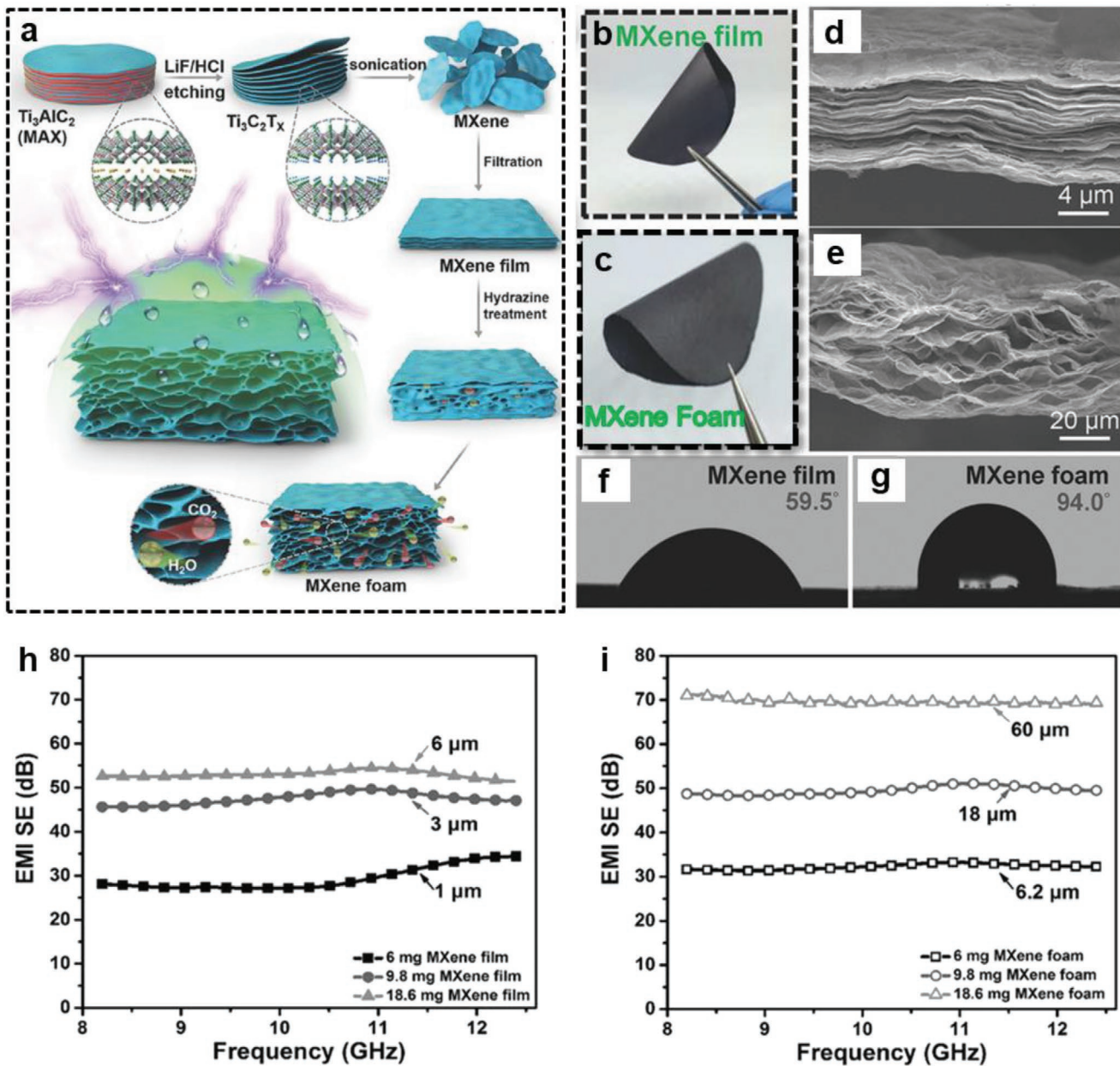


Figure 13. a) The fabrication of the hydrophobic and flexible MXene foam; digital images of the MXene b) film and c) foam; cross-sectional SEM image of the MXene d) film and e) foam; contact angle measurements of the MXene f) film and g) foam; and the EMI SE of the MXene h) films and i) foams of various thicknesses. Adapted with permission.^[70] Copyright 2017, Wiley-VCH.

MXene/protein dispersion with a critical concentration of 2.25 mg mL⁻¹ in DMSO. The EMI SE value of a printed sheet (electrode) with a thickness of 1.35 μm was 50 dB, attributed to its good electrical conductivity of 1080 S cm⁻¹. This technique may be implemented for the development of MXene-based flexible electrodes with customized characteristics.

LbL is applicable to a wide variety of potential candidates with customized chemical, mechanical, and electrical properties. The morphology is crucial for reducing the skin effect in conducting materials,^[69] improving the interaction of EM waves within the layers due to enhanced internal scattering and yielding excellent EMI-shielding capabilities. MXene-based

LbL composites also have good adaptive density, electronic properties, and mechanical strength, which allow for the modification of EMI-shielding efficiency according to obligatory standards.

3.3. Porous MXenes: Foams and Aerogels

Lightweight properties are a perquisite of efficient EMI-shielding materials in aerospace, military, and mobile electronics applications. Porous MXene foams and aerogels are highly suitable due to their extra low density.

Liu et al. reported the first $\text{Ti}_3\text{C}_2\text{T}_x$ MXene foams for lightweight and flexible EMI shielding applications.^[70] Compacted MXene films were immersed in a hydrazine solution at 90 °C. The hydrazine solution infiltrated the MXene layers via capillary action and expanded the MXene stacked sheets to produce a low-density foam structure (Figure 13a–e). Typically, a $\text{Ti}_3\text{C}_2\text{T}_x$ film with a thickness of 1, 3, and 6 μm expanded to 6.2, 18, and 60 μm, respectively. The electrical conductivity of the porous MXene foams were lower (588, 625, and 580 S cm⁻¹, respectively) than the bulk compacted MXene film (4000 S cm⁻¹). Hydrazine reacts with the hydroxyl (−OH) terminations of the MXene, which generates water vapor and releases CO or CO₂ by reducing the C−OH groups in the carbon layers. The reactions with the oxygen-containing groups and the release of gaseous species causes the cellular porous structure. The removal of oxygen terminations during foaming process resulted in larger Ti/O and C/O ratios than the compacted films, which produced an extremely hydrophobic and water resistant surface. The production of hydrophobic MXenes using hydrophilic MXenes also improved the stability against oxidation in humid

environments (Figure 13f,g). Despite their lower electrical conductivities, the porous MXene foams exhibited larger EMI SE values than their bulk counterparts (Figure 13h,i). The EMI SE of the bulk 6 μm thick film increased from 53 to 70 dB after expansion to 60 μm. This considerable improvement in EMI SE was attributed to enhanced internal scattering of the incident EM radiation within the porous MXene foams.

$\text{Ti}_3\text{C}_2\text{T}_x$ MXene/graphene hybrid foams have been designed for EMI shielding applications.^[71] Hybrid foams with varying MXene to GO ratio were produced using simple vacuum drying of frozen solutions at −65 °C followed by thermal reduction at 300 °C for 1 h. The density of a pure rGO foam was 3.1 mg cm⁻³, while the hybrid foam with a MXene to graphene ratio of 1:1 was 7.2 mg cm⁻³. $\text{Ti}_3\text{C}_2\text{T}_x$ MXene has a higher density than graphene, and thus the addition thereof increased the density of the hybrid foam. By increasing the graphene content to 1:2 and 1:3, the density of the hybrid foam was reduced to 4.6 and 3.7 mg cm⁻³, respectively. Similarly, electrical conductivity was significantly improved by adding MXene, and increased from 140 S cm⁻¹ in the rGO foam to 1250 S cm⁻¹. The

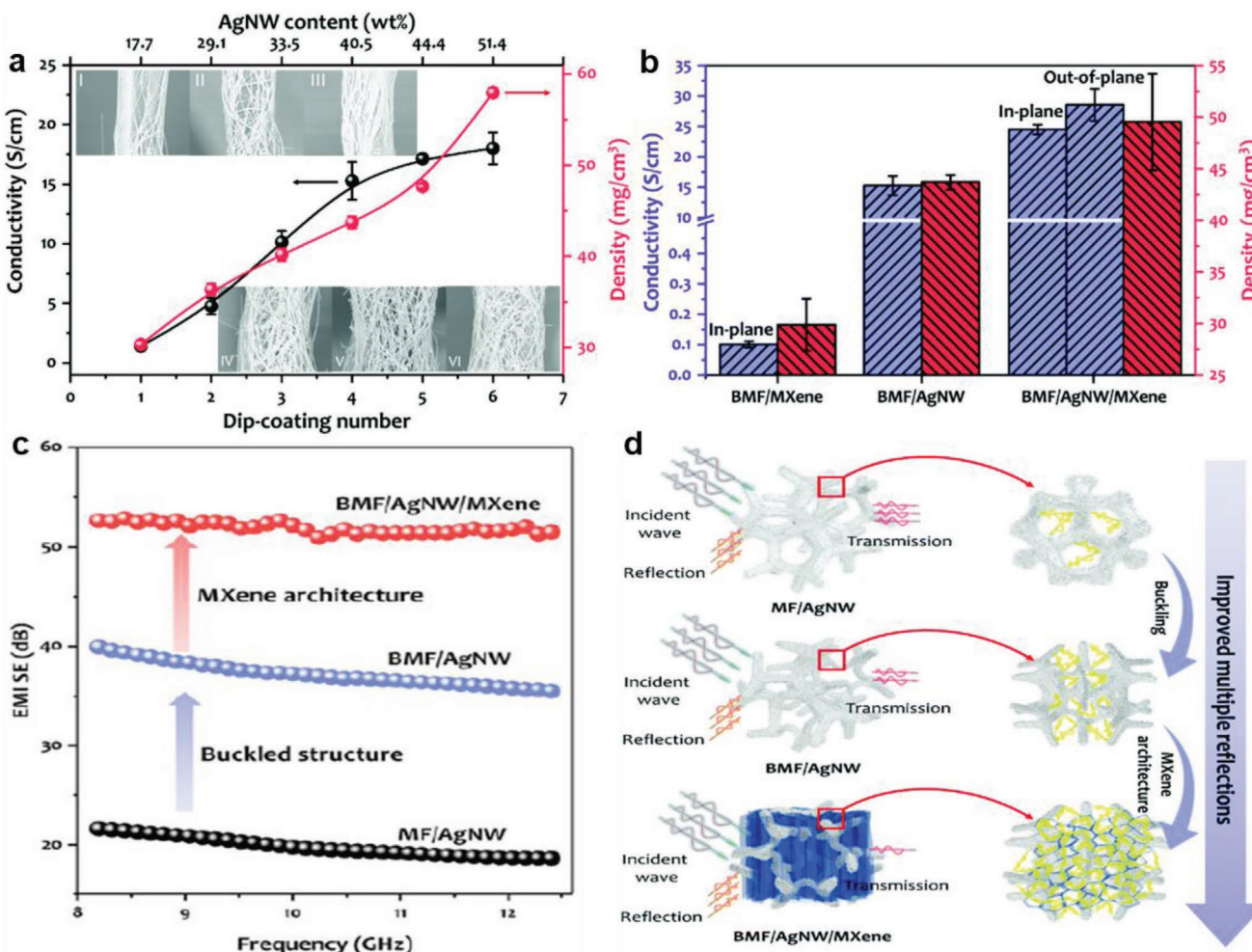


Figure 14. a) Conductivity and mass density of the BMF/AgNW foams at various dip-coating cycles. Inset: SEM images of AgNW-coated backbone of BMF sponge; b) the conductivity and mass density of the BMF/MXene, BMF/AgNW, and BMF/AgNW/MXene foams; c) the EMI SE of the BMF/MXene, BMF/AgNW, and BMF/AgNW/MXene foams; and d) the EMI shielding mechanisms of the MF/AgNW, BMF/AgNW, and BMF/AgNW/MXene foams. Adapted with permission.^[72] Copyright 2019, The Royal Society of Chemistry.

conductive porous structure exhibited enhanced EMI shielding efficiencies and also increased with increase in MXene content. The pure rGO foam exhibited a moderate EMI SE of 15 dB at a thickness of 1.5 mm, and doubled in the 1:1 MXene hybrid. The enhanced EMI shielding efficiency was attributed to internal scattering in highly conductive MXene network. The EMI SE exceeded 50 dB with increase in thickness (3 mm) in the hybrid with a MXene to rGO ratio of 1:2.

The EMI shielding properties of a silver nanowire AgNW/Ti₃C₂T_x MXene hybrid foam have been investigated.^[72] Melamine formaldehyde (MF) porous substrate was uniformly compressed triaxially to produce a buckled melamine formaldehyde (BMF) foam. AgNW was uniformly grown AgNW via repeated dip-coating. The electrical conductivity gradually increased with an increasing number of dip-coating cycles. The conductive foams were immersed in a Ti₃C₂T_x MXene

solution, followed by directional freezing and freeze-drying to produce an irregular honeycomb MXene structure. The BMF/AgNW/Ti₃C₂T_x hybrid composite had a larger electrical conductivity and EMI-shielding properties than separate BMF/AgNW or BMF/MXene composites. The AgNW and Ti₃C₂T_x MXene worked synergistically to yield a higher electrical conductivity in the porous architecture and exhibited superior EMI-shielding efficiency (Figure 14a,c). A 2 mm thick BMF/AgNW/Ti₃C₂T_x hybrid foam with a density of 49.5 mg cm⁻³ exhibited an EMI SE of 52.6 dB, while the BMF/AgNW and BMF/MXene foams were both 40 dB. The enhanced shielding behavior was attributed to improved electrical conductivity, which led to an impedance mismatch between the hybrid and the vacant spaces. Furthermore, internal scattering of the incident EM waves from conductive porous interfaces was increased, which resulted in absorption dominant EMI shielding.

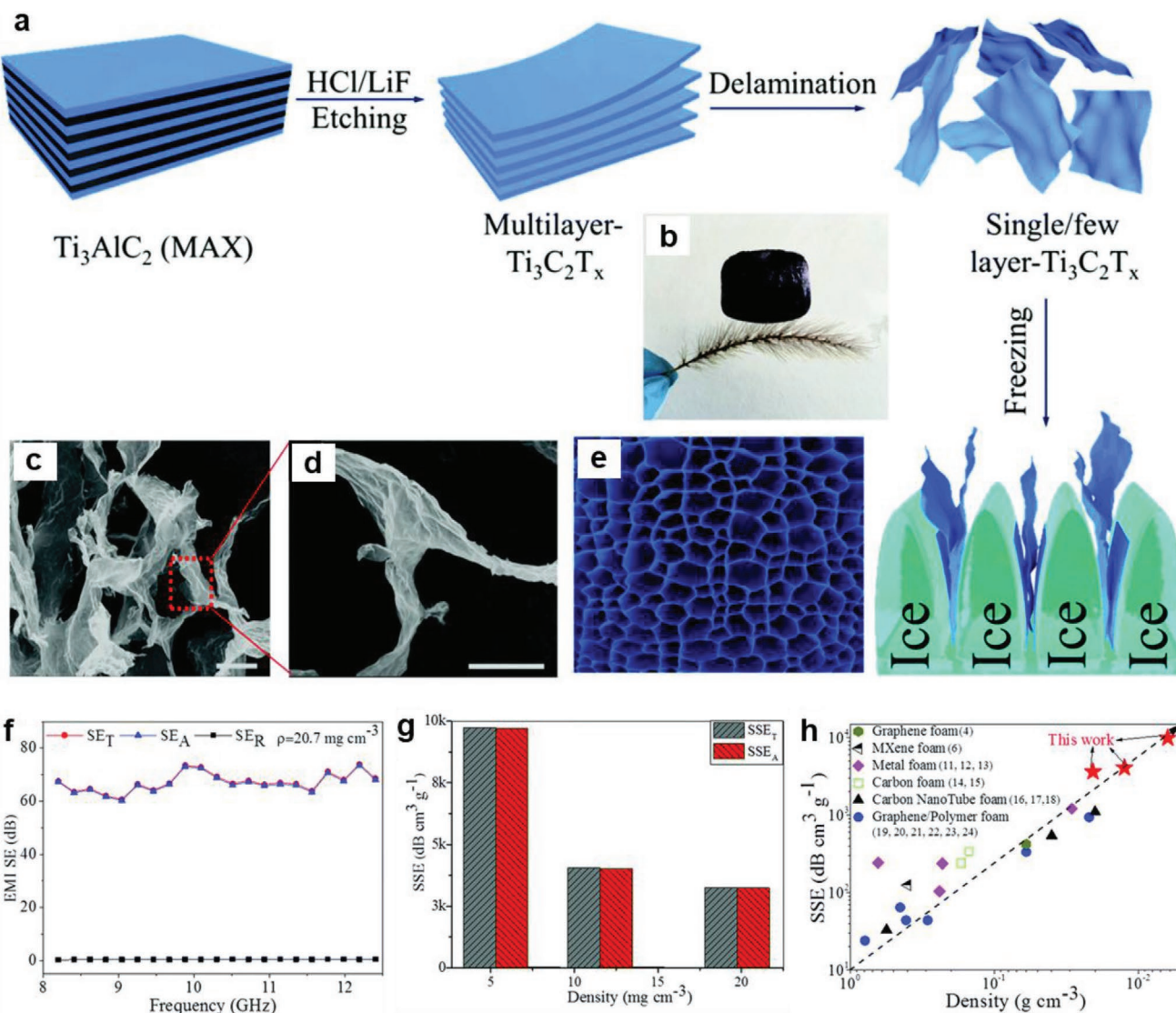


Figure 15. a) The fabrication of the Ti₃C₂T_x MXene aerogel; b,c) SEM images of the MXene aerogel at different magnifications (scale bar = 10 mm); d) the top view of resultant MXene aerogel; e) the incredibly light MXene aerogel (35 cm³) placed on a foxtail grass; f) the EMI of the MXene aerogel with a density of 20.7 mg cm⁻³; g) the SE_T and SE_A of the MXene aerogel; and h) comparison of specific shielding as a function of density for various foam-like materials. Adapted with permission.^[77] Copyright 2019, The Royal Society of Chemistry.

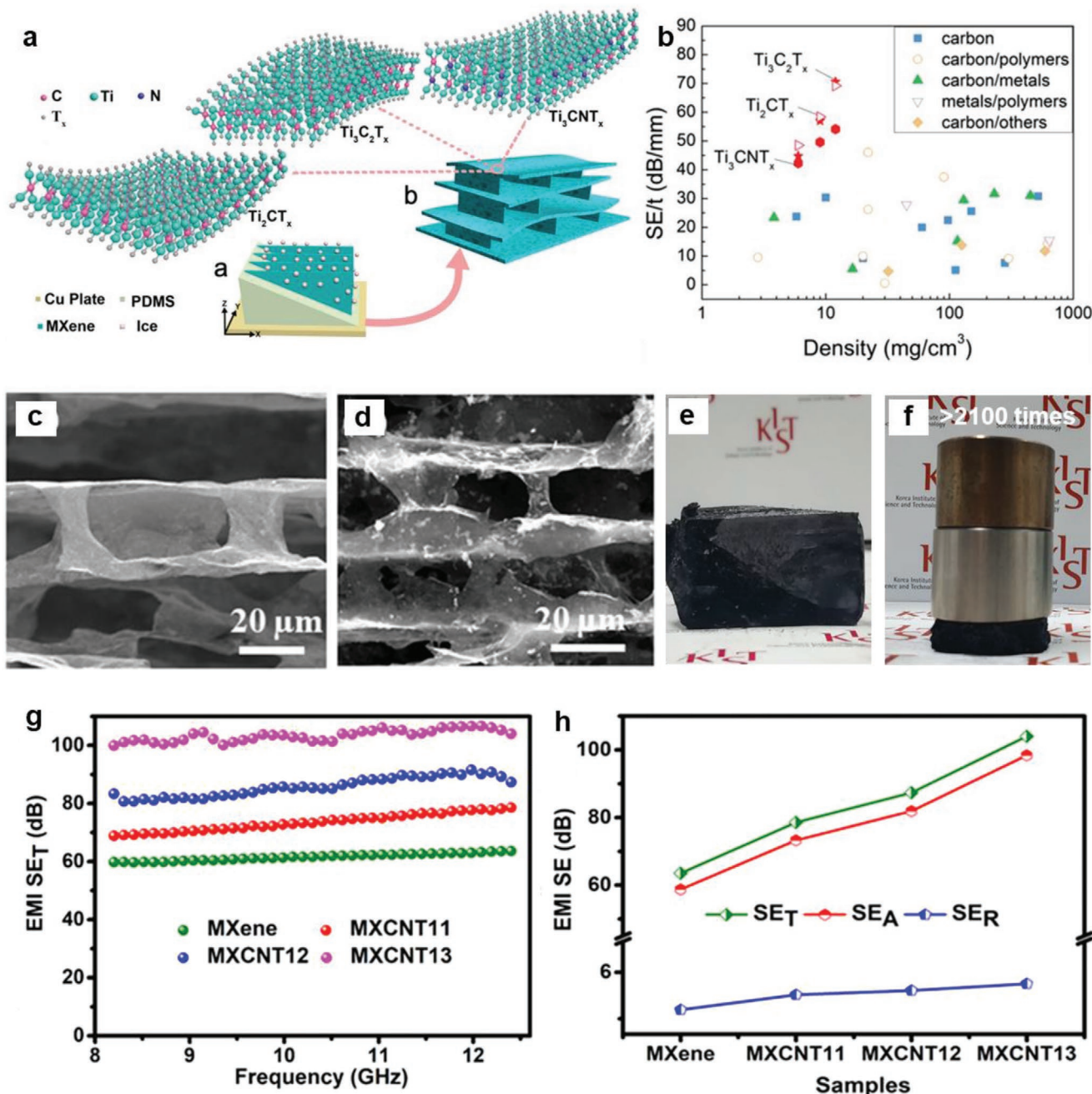


Figure 16. a) Bidirectional freeze-casting mechanism; b) the proposed EMI shielding mechanism in the 3D porous structures; the SEM images of c) pure Ti₃C₂T_x MXene and d) MXCNT13 aerogels; the MXCNT13 aerogel e) before and f) during compression; g) the total EMI SE of the Ti₃C₂T_x/CNTs aerogels; and h) the absolute EMI SET, SER, and SEA of the Ti₃C₂T_x/CNTs aerogels at 12.4 GHz. a,b) Adapted with permission.^[37] Copyright 2019, Wiley-VCH. c-h) Adapted with permission.^[78] Copyright 2019, American Chemical Society.

A compressible and durable Ti₃C₂T_x MXene/sodium alginate/polydimethylsiloxane (MXene/SA/PDMS) hybrid foam has been formed using a simple freezing and freeze-drying method.^[73] A 2 mm thick lightweight MXene/SA foam with 95% MXene has a density of ≈ 20 mg cm⁻³, an electrical conductivity of 22.11 S cm⁻¹, and excellent EMI SE of 72 dB. A thin coating of PDMS was applied onto the MXene/SA foam through vacuum filtration, and the EMI shielding efficiency decreased slightly to 50 dB. However, the coating enhanced

the structural stability and durability and the MXene/SA/PDMS hybrid foam retained its EMI-shielding efficiency over 500 bending and compressing cycles. The role of the porous architecture in EM radiation attenuation was highlighted when the hybrid foam was compared with a simple blend of MXene/SA/PDMS and a MXene/SA foam coated with a solid PDMS layer that covered all of the pores. The MXene/SA/PDMS hybrid foam with a thin uniform PDMS coating exhibited the highest EMI SE of 54 dB, followed by the foam with

a solid PDMS coating (50 dB) and the simple blended composite (9 dB).

A mechanically strong epoxy was impregnated into a $\text{Ti}_3\text{C}_2\text{T}_x$ MXene/carbon hybrid foam using a sol-gel and thermal reduction method.^[74] Resorcinol, formaldehyde, and a sodium carbonate catalyst were added to a 10 mL $\text{Ti}_3\text{C}_2\text{T}_x$ MXene dispersion, sonicated, cured at 90 °C for 5 h under nitrogen and freeze-dried. The porous foam was annealed at 400 °C for 2 h to produce the MXene/carbon hybrid foam. An epoxy solution was impregnated into the porous hybrid foam under vacuum. The MXene/carbon foam had a combined content of 4.25 wt% (1.64 wt% MXene and 2.61 wt% carbon) in the epoxy and exhibited an electrical conductivity of 1.84 S cm⁻¹ and EMI SE of 46 dB across the full X-band frequency range at a thickness of 2 mm. An increased MXene content resulted in a hardness of 0.31 GPa and Young's modulus of 3.96 GPa, which was higher than that of the pure carbon/epoxy composites (0.28 GPa, and 3.51 GPa, respectively). Conductive 2D MXene flakes have a major effect on electrical, mechanical, and the EMI-shielding properties of epoxy-based composites and hybrid foams.

Ti_2CT_x MXene/PVA composite foams with low reflection were evaluated for EMI-shielding applications.^[75] The Ti_2CT_x /PVA foam was produced using a simple free-drying method. Strong hydrogen bonding between the surface terminations of MXene and the PVA molecular chains imparted extra flexibility and robust mechanical strength. While the Ti_2CT_x /PVA composite foam had a lower electrical conductivity than porous $\text{Ti}_3\text{C}_2\text{T}_x$, it was much higher than other carbon based materials.^[76] A 5 mm thick Ti_2CT_x /PVA foam with a density of 10.9 mg cm⁻³ exhibited an EMI SE ranging from 26 to 33 dB. The low density of the compressed foam structure contributed to an SSE/t of 5136 dB cm² g⁻¹ at a very low content of Ti_2CT_x .

MXene (0.15 vol%). The porous foam absorbed incident EM waves more efficiently than a compact film structure, where EM waves entered the shield and strong internal scattering caused the dissipation of energy as heat. Dielectric and interfacial polarization from an alternating EM field also contributed toward the absorption of EM radiation.

A $\text{Ti}_3\text{C}_2\text{T}_x$ MXene-based aerogel was produced using conventional freeze-drying of MXene dispersions with different concentrations (Figure 15).^[77] The aerogel density was controlled by the concentration of the MXene solution used during freeze drying, while the morphology of the pores was determined by the ice crystals formed during freezing. The $\text{Ti}_3\text{C}_2\text{T}_x$ MXene aerogels had a particularly low density of 20.7 mg cm⁻³, but were dimensionally stable and exhibited an electrical conductivity of 22 S cm⁻¹ and EMI shielding of 75 dB. At 2 mm thickness, the SSE/t value was 18 116 dB cm² g⁻¹.

Aerogels using three different MXenes ($\text{Ti}_3\text{C}_2\text{T}_x$, Ti_3CNT_x , and Ti_2CT_x) have been compared (Figure 16a,b).^[37] Flexible aerogels were produced using bidirectional freeze drying of MXenes solutions with varying concentrations. Aerogels with long range aligned lamellar structures were obtained, which is not possible via a conventional freeze drying method. The highly conductive MXene-based framework comprised of a porous architecture with MXene sheets as connecting bridges. Solutions with a higher concentration of MXenes (e.g., 11 mg mL⁻¹) formed more conductive and durable structures. The electrical conductivities of the $\text{Ti}_3\text{C}_2\text{T}_x$, Ti_3CNT_x , and Ti_2CT_x aerogels were higher than other carbon materials, resulting in larger EMI SE and SE/t values (Figure 16b). The average total EMI SE (SE_T) values of $\text{Ti}_3\text{C}_2\text{T}_x$, Ti_3CNT_x , and Ti_2CT_x aerogels were 70.5, 69.2, and 54.1 dB, respectively, in the X band frequency range at a thickness of 1 mm.

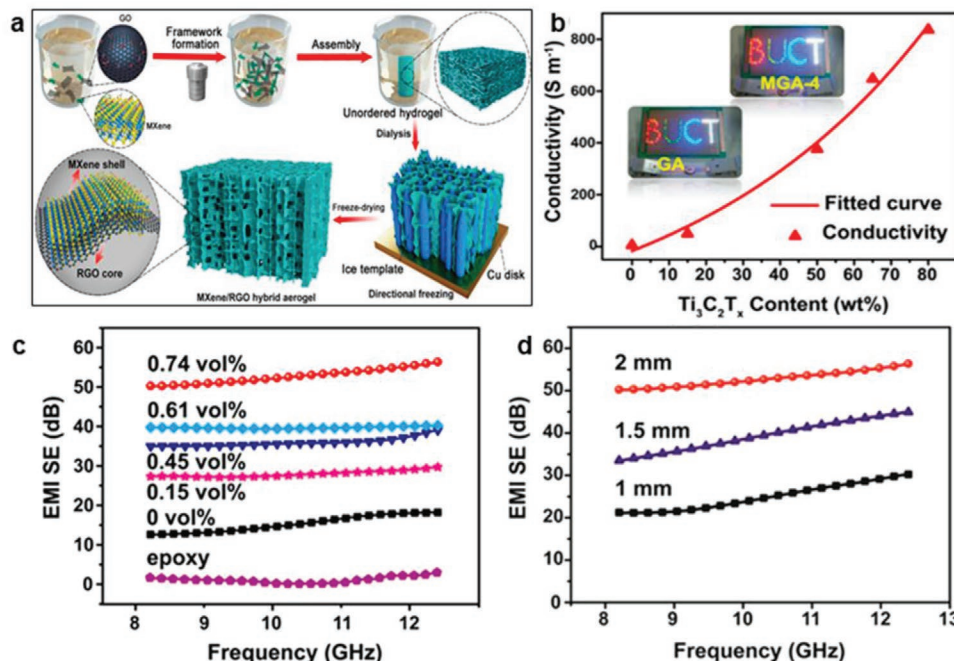


Figure 17. a) The synthesis of a $\text{Ti}_3\text{C}_2\text{T}_x$ MXene/rGO hybrid aerogel; b) the electrical conductivity values of hybrid aerogels with varying MXene contents; and the EMI SE of hybrid aerogels with varying c) MXene contents and d) thicknesses. Adapted with permission.^[79] Copyright 2018, American Chemical Society.

MXene/CNT hybrid (MXCNT) aerogels were synthesized by reinforcing mechanically strong $\text{Ti}_3\text{C}_2\text{T}_x$ MXene with 1D conductive CNTs (Figure 16c,d).^[78] The highly conductive CNTs supported the MXene bridges in the alternating layers and synergistically improved the electrical conductivity and mechanical properties of the aerogel. Compression testing of the MXCNTs aerogels demonstrated improved compressive strength compared to that of pure $\text{Ti}_3\text{C}_2\text{T}_x$ MXene (Figure 16e,f). The compression moduli of the $\text{Ti}_3\text{C}_2\text{T}_x$ aerogels with varying CNT weight ratios (1:1, 1:2, and 1:3) increased by 3898, 7796, and 9661%, respectively, in comparison with the pure $\text{Ti}_3\text{C}_2\text{T}_x$ MXene aerogel. A maximum EMI SE value of over 100 dB was achieved in the 3 mm thick MXCNT13 aerogel that had an MXene to CNT weight ratio of 1:3 (Figure 16g), where the SSE/t value reached 8253.9 dB cm² g⁻¹. The porous structure allowed for absorption-dominant EMI-shielding behavior in the $\text{Ti}_3\text{C}_2\text{T}_x$ /CNT aerogels (Figure 16h). This shielding mechanism was governed by three factors, namely electron migration due to the electric field of the EM waves, dipolar polarization

due to surface terminations, and internal scattering in the porous architecture. The mechanically robust $\text{Ti}_3\text{C}_2\text{T}_x$ /CNTs aerogels are a promising solution for lightweight EMI-shielding applications.

Similarly, $\text{Ti}_3\text{C}_2\text{T}_x$ MXene/reduced graphene oxide (MXene/rGO) aerogels were synthesized using directional freezing and freeze-drying to improve the dimensional stability of a MXene aerogel (Figure 17a).^[79] A highly compacted aligned cellular structure was obtained in which the conductive $\text{Ti}_3\text{C}_2\text{T}_x$ MXene sheets covered the graphene sheet shell. The larger sheet size of rGO enhanced the mechanical stability of the framework, while the highly conductive MXene sheets contributed to the excellent conductivity of the porous structure (Figure 17b). At a very low $\text{Ti}_3\text{C}_2\text{T}_x$ MXene content of 0.74 vol%, an electrical conductivity of 10.85 S cm⁻¹ and EMI SE of 50 dB was achieved in a 2 mm thick foam (Figure 17c,d). The EM radiation entering the porous materials was internally scattered due to large surface area and multiple interfaces, which lead to either attenuation or dissipation as heat. Surface terminations and the structural

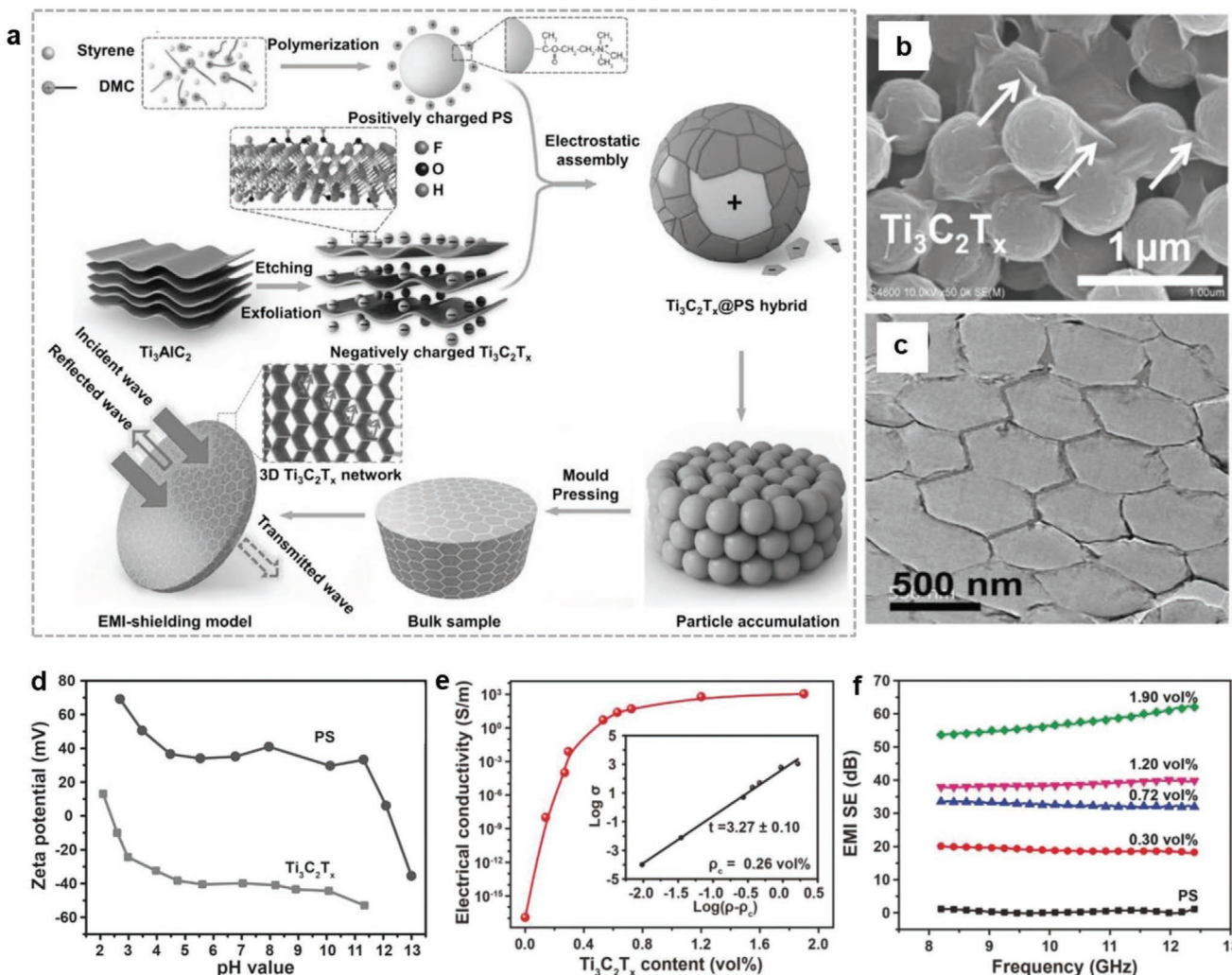


Figure 18. a) The fabrication of the $\text{Ti}_3\text{C}_2\text{T}_x$ @PS nanocomposites; the b) SEM and c) TEM images of the $\text{Ti}_3\text{C}_2\text{T}_x$ @PS-570 hybrid with 1.20 vol% $\text{Ti}_3\text{C}_2\text{T}_x$; d) the zeta potentials of positively charged PS microspheres and negatively charged $\text{Ti}_3\text{C}_2\text{T}_x$ nanosheets; and the e) electrical conductivity and f) EMI SE of the $\text{Ti}_3\text{C}_2\text{T}_x$ @PS-570 nanocomposites. Adapted with permission.^[81] Copyright 2017, Wiley-VCH.

defects contributed to the absorption of EM waves via dielectric polarization loss. Consequently, the EM radiation absorption loss within the shield increased.

$\text{Ti}_3\text{C}_2\text{T}_x$ /calcium alginate (MXene/CA) aerogel films were prepared via divalent calcium-ion-induced crosslinking, followed by vacuum filtration and freeze-drying.^[80] The sponge like structure improved the EMI shielding ability due to internal reflections by multiple scattering sites and interfaces. A 26 μm thick MXene/CA aerogel with 90 wt% MXene exhibited an EMI SE of 54.3 dB and a specific EMI shielding of 17 586 dB $\text{cm}^2 \text{g}^{-1}$.

The porous structure of foams and aerogels produces additional interfaces for internal scattering that spreads incident EM radiation throughout the shield, resulting in extra attenuation due to absorption. The terminations on the surface of MXene also enhance the absorption of EM waves via dipole polarization losses. The proposed mechanism for the interaction between EM waves and the foam or aerogel is detailed in Figure 2c. MXene foams and aerogels with a low density and good mechanical stability are optimal candidate for use

as lightweight EMI-shielding materials in military, radar, and stealth technology applications.

3.4. MXenes' Segregated Structures

Polymer composites with high electrical conductivity require larger conducting filler volumes, which can render the production costly and complex. A segregated structure is a multiphase structure wherein conductive fillers are segregated to form a conducting network at low volume fraction within an insulating polymer matrix.^[81,82] This inter-connected network of conductive fillers improves the electronic and mechanical properties of the structure and can enhance the shielding capability even at low concentrations.

Highly conductive $\text{Ti}_3\text{C}_2\text{T}_x$ MXene@polystyrene (PS) nanocomposites were synthesized with a very low MXene content (Figure 18a–c).^[81] The electrostatic assembly included positively charged PS beads of different diameters (80, 310, and 570 μm) uniformly coated with negatively charged $\text{Ti}_3\text{C}_2\text{T}_x$

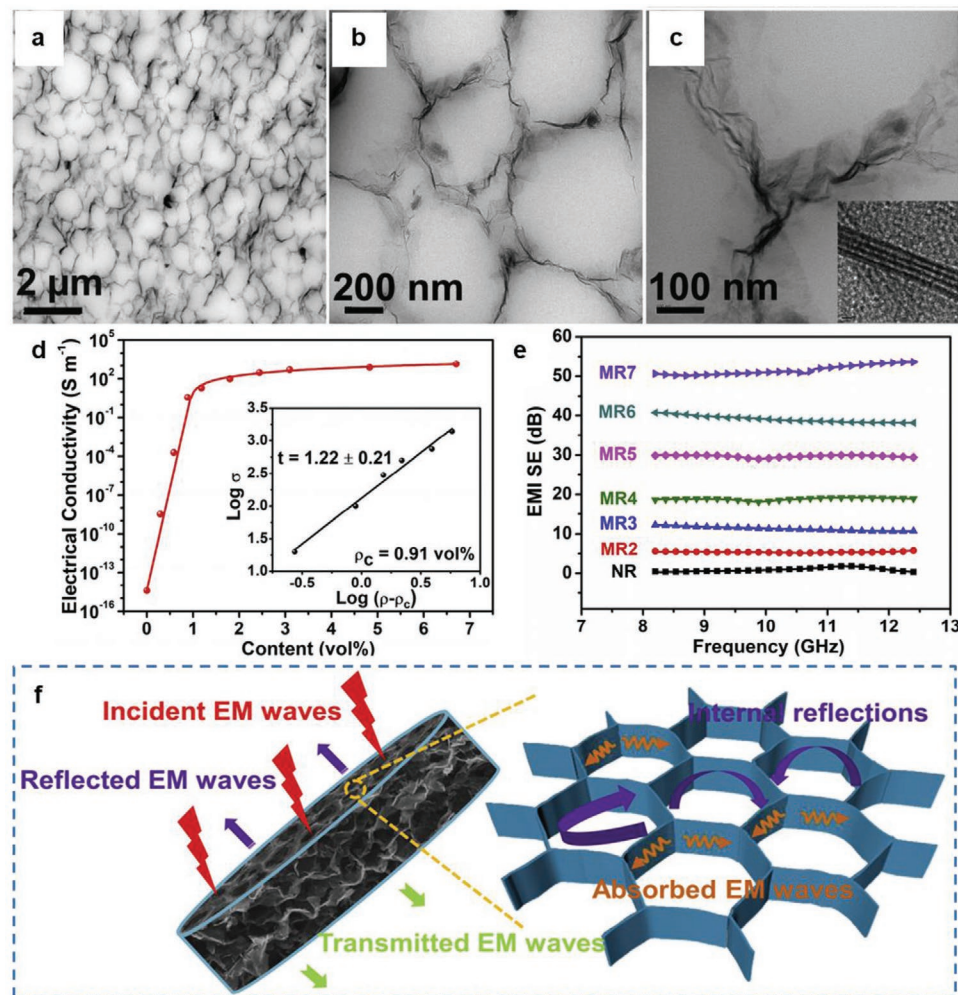


Figure 19. a–c) TEM images of MXene-NR (MR5) nanocomposite (inset: HRTEM of MXene sheets); the d) electrical conductivity and e) EMI SE of MXene-NR nanocomposites at different MXene loadings, where x is an integer in $\text{MR}x$ to represent volume percentage of MXene; and f) the EMI shielding mechanism in the nanocomposite with a continuous MXene network. Adapted with permission.^[82] Copyright 2019, Elsevier.

MXene sheets (zeta potential = approx. -40 mV) (Figure 18d). The $\text{Ti}_3\text{C}_2\text{T}_x$ -coated PS beads were vacuum filtered, dried, and compressed at 130 °C for 30 min to obtain $\text{Ti}_3\text{C}_2\text{T}_x@$ PS nanocomposite films. As predicted by the power law, the electrical conductivity rapidly increased with increase in the $\text{Ti}_3\text{C}_2\text{T}_x$ volume fraction. Furthermore, the segregated structure of the $\text{Ti}_3\text{C}_2\text{T}_x@$ PS nanocomposites, which included continuous conductive channels (electrical contacts) between the MXene sheets, allowed for a large electrical conductivity at a very low volume fraction of MXene (0.26 vol%). When the MXene content was increased, the $\text{Ti}_3\text{C}_2\text{T}_x@$ PS nanocomposite exhibited an electrical conductivity of 6.02 and 10.81 S cm^{-1} at 1.20 and 1.90 vol%, respectively (Figure 18e). This increased electrical conductivity positively impacted the EMI shielding of the MXene–polymer composite, and the shielding efficiency at 2 mm thickness increased linearly with increase in MXene content to a maximum value of over 60 dB at 1.90 vol% (Figure 18f).

A highly flexible and stretchable $\text{Ti}_3\text{C}_2\text{T}_x$ MXene/natural rubber (NR) nanocomposite film was produced using simple vacuum filtration with varying concentrations of MXene.^[82] The electrostatic repulsion between the negatively charged MXene sheets and NR latex ensured even distribution of the MXene sheets between the NR particles to form a continuous interconnected conductive 3D MXene network in the NR matrix (Figure 19a–c). A large electrical conductivity (14 S cm^{-1}) was measured in the nanocomposites with lower MXene content (Figure 19d). The EMI shielding increased with increase in conductive MXene content, and the segregated structure of a $250 \mu\text{m}$ thick MXene–NR composite exhibited an excellent

EMI SE of 53.6 dB at 6.7 vol% MXene (Figure 19e). The conductive network attenuated the incident EM energy through the flow of electrons and internal scattering at the numerous interfaces.

4. Summary and Perspectives

The field of EMI shielding was revolutionized in 2016 by the first application of MXenes. An array of reports on “2D MXenes; shields against EMI” have since been published. Based on the published literature, the different structural forms including compact and laminate structures, layer-by-layer assemblies, porous foams, and aerogels, and segregated structures have been evaluated according to various controlling factors, such as thickness, density, and EMI SE (Figure 20). Summarized EMI SE of MXene-based shielding materials in different structural forms and their corresponding composition, thickness, density, and the absolute shielding effectiveness (SSE/t) have been given in Figure 20 and Table 1. When a thin shield is required, such as in miniaturized electronics, compact MXene laminates, and their composites are ideal ultrathin shielding materials with superb mechanical properties (Figure 20a). MXene laminates provide better EMI SE with a comparatively small thickness, and can be produced at a nanoscale to meet the requirements of commercial products. The porous foams and aerogels offer strong ultra-lightweight EMI shielding at the expense of the thickness that is advantageous for the aerospace and military applications (Figure 20b). A tradeoff between density and the thickness for efficient EMI shielding is inevitable, but a suitable

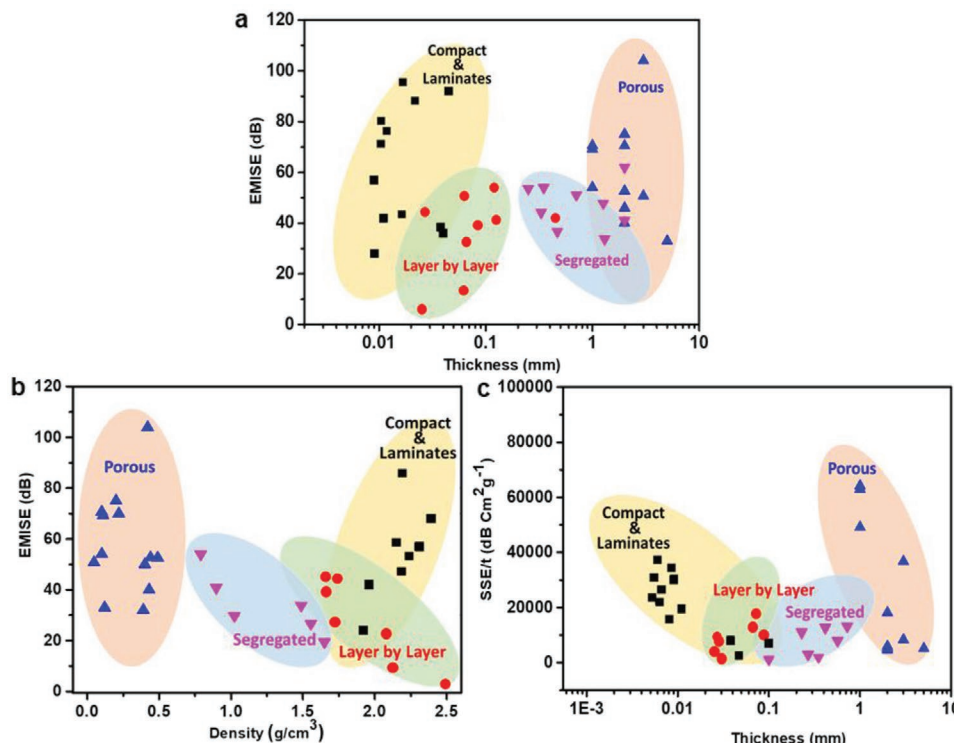


Figure 20. A comprehensive summary data displayed as EMI SE of MXene-based different structures as a function of a) thickness and b) density, and c) absolute shielding effectiveness (SSE/t) as a function of thickness.

Table 1. EMI shielding performance of various structural forms based on MXenes.

	Sr. #	Composition	Density [g cm ⁻³]	Thickness [mm]	SE [dB]	SSE/t [dB cm ² g ⁻¹]	Ref
Compact & laminates structures	1.	Ti ₃ C ₂ T _x	2.39	0.045	92	8554	[1]
	2.	Ti ₃ C ₂ T _x /SA	2.11	0.009	57	30015	
	3.	Ti ₃ C ₂ T _x /SiO ₂	/	1	58	/	[44]
	4.	Ti ₃ C ₂ T _x /Wax	2.03	0.8	70	1776	[45]
	5.	Ti ₃ C ₂ T _x /CNF	1.92	0.047	24	2647	[47]
	6.	Ti ₃ C ₂ T _x /CNF/CNT	1.26	0.038	38.4	8020	[48]
	7.	Ti ₃ C ₂ T _x /HEC	0.34	0.1	24	7000	[49]
	8.	Ti ₃ C ₂ T _x /ANF	1.25	0.017	33	15529	[50]
	9.	Ti ₃ C ₂ T _x /epoxy	/	2	41	/	[51]
	10.	Ti ₃ C ₂ T _x /PEDOT:PSS	1.96	0.011	42.1	19497	[52]
	11.	Ti ₃ C ₂ T _x /PANI	/	0.04	36	/	[53]
	12.	Ti ₃ C ₂ T _x /TiO ₂ /rGO	1.01	0.009	28	30293	[54]
	13.	Ti ₃ C ₂ T _x /rGO/PVDF	0.79	0.35	54	1944	[55]
	14.	Ti ₃ C ₂ T _x /Ni/PVDF	1.65	0.10	19.5	1177	[56]
	15.	Ti ₃ C ₂ T _x /Ni	/	1.3	33.8	/	[57]
Layer-by-layer	16.	Ti ₃ C ₂ T _x /CNT	2.49	0.0002	2.9	58187	[64]
	17.	Ti ₃ C ₂ T _x /PVA	1.74	0.027	44.4	9343	[65]
	18.	Ti ₃ C ₂ T _x /AgNW	/	0.120	54	/	[66]
	19.	Ti ₃ C ₂ T _x /PPy	/	0.45	42	/	[67]
	20.	Ti ₃ C ₂ T _x /PPy	/	1.3	90	/	[67]
	21.	Ti ₃ C ₂ T _x /TR42	/	1.35	50	/	[68]
Porous	22.	Ti ₃ C ₂ T _x	0.109	1	70.6	64182	[37]
	23.	Ti ₃ CNT _x	0.11	1	69.2	62909	[37]
	24.	Ti ₂ CT _x	0.109	1	54.1	49182	[37]
	25.	Ti ₃ C ₂ T _x foam	0.39	0.006	32	136752	[70]
	26.	Ti ₃ C ₂ T _x foam	0.40	0.018	50	69444	[70]
	27.	Ti ₃ C ₂ T _x foam	0.22	0.06	70	53030	[70]
	28.	Ti ₃ C ₂ T _x /rGO	0.046	3	50.7	36737	[71]
	29.	Ti ₃ C ₂ T _x /AgNW	0.49	2	52.6	5313	[72]
	30.	Ti ₃ C ₂ T _x /AgNW	0.43	2	40	4650	[72]
	31.	Ti ₃ C ₂ T _x /SA/PDMS	0.02	2	72	18000	[73]
	32.	Ti ₃ C ₂ T _x /carbon	/	2	46	/	[74]
	33.	Ti ₃ C ₂ T _x /PVA	0.128	5	33	5136	[75]
	34.	Ti ₃ C ₂ T _x	0.206	2	75	18116	[77]
	35.	Ti ₃ C ₂ T _x /CNT	0.42	3	104	8253	[78]
	36.	Ti ₃ C ₂ T _x /rGO	0.44	2	52.7	5988	[79]
	37.	Ti ₃ C ₂ T _x /CA	1.18	0.026	54.3	17586	[80]
Segregated	38.	Ti ₃ C ₂ T _x /PS	/	2	62	/	[81]
	39.	Ti ₃ C ₂ T _x /NR	/	0.25	53.6	/	[82]

SA, sodium alginate; CNT, carbon nanotube; CNF, cellulose nanofiber; ANF, aramid nanofiber; HEC, hydroxyethyl cellulose; PEDOT:PSS, poly(3,4-ethylenedioxythiophene):poly(styrenesulfonate); PANI, polyaniline; rGO, reduced graphene oxide; PVDF, polyvinylidene difluoride; PVA, poly(vinyl alcohol); NW, nanowires; PPy, polypyrrole; PDMS, polydimethylsiloxane; CA, calcium alginate; PS, polystyrene; NR, natural rubber.

combination of both can provide excellent absolute shielding effectiveness (SSE/t). Porous foam and aerogel structures offer the largest SSE/t value, while laminate structures offer larger SSE/t values than layer-by-layer morphology and segregated structures (Figure 20c). The segregated structures with

extremely low MXene loadings make themselves very cost-effective. Thus, this review demonstrates that the wide variety of MXene-based shield structures allow one to consider all aspects of an application for the practical implementation in a specified field.

State-of-the art EMI shielding performance is given by $Ti_3C_2T_x$ due to its excellent metallic conductivity where it outperformed all other conducting materials and their composites at comparable thickness values. Yet, some challenges exist there in the MXenes system to be considered for the future study. Most of all, despite the fact that synthesis methods for more than 30 different MXenes have been reported, few MXenes including Ti_3C_2 , Ti_2C , Mo_2TiC_2 , $Mo_2Ti_2C_3$, and Ti_3CN have been investigated. Other MXenes need to be explored to understand the effects of elemental composition, layered structure, and transition metal arrangement on EMI shielding properties of MXenes. Additionally, being a large family, MXenes with new atomic compositions or new crystal structure like M_5X_4 are possible to be synthesized and studied. Normally, the highly conductive MXenes show large reflection contribution to the EMI shielding which may cause secondary pollution. To combat this, structural designs have been suggested like porous foams and aerogels, and the segregated structures; however, it is still needed to develop the MXene-shielding materials with different structural factor like meta-structure that may significantly improve the absorption of the incident EM waves. Additionally, the hydrophilic nature of MXenes is limited to making their polymer composites or hybrids with other nanomaterials only in aqueous systems. However, in order to widen the window of structural design, it is necessary to synthesize and study the MXenes having surface hydrophobicity and their organic dispersions.

The study of MXenes is still in its infancy and there is a large space available to explore more about the new MXenes and their shielding capability. We hope that this comprehensive review provides an insight into future challenges and guidelines for finding material solutions for next-generation shielding applications.

Acknowledgements

A.I. and P.S. contributed equally to this work. This work was supported by a grant from the Basic Science Research Program (2017R1A2B3006469) through the National Research Foundation of Korea funded by the Ministry of Science, ICT and Future Planning, the Fundamental R&D Program (I0077545) for Core Technology of Materials and the Industrial Strategic Technology Development Program funded by the Ministry of Knowledge Economy, and Construction Technology Research Project (I9SCIP-B146646-02) funded by Ministry of Land, Infrastructure and Transport, Republic of Korea. C.M.K. also acknowledges KIST and KU-KIST internal programs.

Conflict of Interest

The authors declare no conflict of interest.

Keywords

electromagnetic interference shielding, shielding mechanisms, internal scattering, MXenes, structure design

Received: January 30, 2020

Revised: March 13, 2020

Published online:

- [1] F. Shahzad, M. Alhabeb, C. B. Hatter, B. Anasori, S. M. Hong, C. M. Koo, Y. Gogotsi, *Science* **2016**, *353*, 1137.
- [2] T. Yun, H. Kim, A. Iqbal, Y. S. Cho, G. S. Lee, M.-K. Kim, S. J. Kim, D. Kim, Y. Gogotsi, S. O. Kim, C. M. Koo, *Adv. Mater.* **2020**, *32*, 1906769.
- [3] Z. Chen, C. Xu, C. Ma, W. Ren, H.-M. Cheng, *Adv. Mater.* **2013**, *25*, 1296.
- [4] P. Sambyal, A. P. Singh, M. Verma, M. Farukh, B. P. Singh, S. K. Dhawan, *RSC Adv.* **2014**, *4*, 12614.
- [5] G. Redlarski, B. Lewczuk, A. Źak, A. Koncicki, M. Krawczuk, J. Piechocki, K. Jakubiuk, P. Tojza, J. Jaworski, D. Ambroziak, Ł. Skarbek, D. Gradolewski, *Biomed Res. Int.* **2015**, *2015*, 234098.
- [6] R. Starn, S. Yamaguchi-Sekino, *Ind. Health* **2018**, *56*, 96.
- [7] A. Christ, M. Douglas, J. Nadakuduti, N. Kuster, *Proc. IEEE* **2013**, *101*, 1482.
- [8] O. Carpenter David, *Rev. Environ. Health* **2013**, *28*, 159.
- [9] B. Hocking, K. H. Mild, *Int. J. Occup. Saf. Ergon.* **2008**, *14*, 217.
- [10] W. Irnich, J. M. T. de Bakker, H.-J. Bisping, *Pacing Clin. Electrophysiol.* **1978**, *1*, 52.
- [11] Y. Kawamura, T. Hikage, T. Nojima, K. Fukui, H. Fujimoto, T. Toyoshima, *Trans. Japan. Soc. Med. Biol. Engine.* **2012**, *50*, 289.
- [12] J. P. Thaker, M. B. Patel, K. Jongnarangsin, V. V. Liepa, R. K. Thakur, *Heart Rhythm* **2008**, *5*, 538.
- [13] G. Calcagnini, P. Bartolini, M. Floris, M. Triventi, P. Cianfanelli, G. Scavino, L. Proietti, V. Barbaro, presented at The 26th Annual Int. Conf. of the IEEE Engineering in Medicine and Biology Society, September **2004**.
- [14] G. Nimtz, U. Panten, *Ann. Phys.* **2010**, *19*, 53.
- [15] Y.-S. Choi, Y.-H. Yoo, J.-G. Kim, S.-H. Kim, *Surf. Coat. Technol.* **2006**, *201*, 3775.
- [16] L. De Temmerman, *J. Coated Fabr.* **1992**, *21*, 191.
- [17] S. Geetha, K. Sathesh Kumar, C. R. Rao, M. Vijayan, D. Trivedi, *J. Appl. Polym. Sci.* **2009**, *112*, 2073.
- [18] X. Luo, D. Chung, *Composites, Part B* **1999**, *30*, 227.
- [19] M. Jaroszewski, S. Thomas, A. V. Rane, *Advanced Materials for Electromagnetic Shielding: Fundamentals, Properties, and Applications*, John Wiley & Sons, New York **2018**.
- [20] P. Saini, M. Arora, *New Polym. Spec. Appl.* **2012**, *3*, 73.
- [21] S. Sankaran, K. Deshmukh, M. B. Ahamed, S. K. Khadheer Pasha, *Composites, Part A* **2018**, *114*, 49.
- [22] D. Jiang, V. Murugadoss, Y. Wang, J. Lin, T. Ding, Z. Wang, Q. Shao, C. Wang, H. Liu, N. Lu, *Polym. Rev.* **2019**, *59*, 280.
- [23] F. Shahzad, C. M. Koo, in *Handbook of Graphene Set* **2019**, Vol. 1, p. 663.
- [24] M. Naguib, V. N. Mochalin, M. W. Barsoum, Y. Gogotsi, *Adv. Mater.* **2014**, *26*, 992.
- [25] M. Naguib, M. Kurtoglu, V. Presser, J. Lu, J. Niu, M. Heon, L. Hultman, Y. Gogotsi, M. W. Barsoum, *Adv. Mater.* **2011**, *23*, 4248.
- [26] M. Alhabeb, K. Maleski, B. Anasori, P. Lelyukh, L. Clark, S. Sin, Y. Gogotsi, *Chem. Mater.* **2017**, *29*, 7633.
- [27] H. W. Ott, *Electromagnetic Compatibility Engineering*, John Wiley & Sons, New York **2011**.
- [28] B. Anasori, Y. Gogotsi, *2D Metal Carbides and Nitrides (MXenes): Structure, Properties and Applications*, Springer International Publishing, New York **2019**.
- [29] S. Schelkunoff, *Electromagnetic Waves*, Princeton, NJ **1943**.
- [30] R. B. Schulz, V. Plantz, D. Brush, *IEEE Trans. Electromagn. Compat.* **1988**, *30*, 187.
- [31] P. Modak, D. Nandanwar, *Int. J. Adv. Sci. Eng. Technol.* **2015**, *1*, 212.
- [32] A. Joshi, S. Datar, *Pramana* **2015**, *84*, 1099.
- [33] A. P. Singh, M. Mishra, P. Sambyal, B. K. Gupta, B. P. Singh, A. Chandra, S. Dhawan, *J. Mater. Chem. A* **2014**, *2*, 3581.
- [34] K. L. Kaiser, *Electromagnetic Shielding*, CRC Press, Boca Raton, FL **2005**.

- [35] N. Sohi, M. Rahaman, D. Khastgir, *Polym. Compos.* **2011**, *32*, 1148.
- [36] R. Kumar, H. K. Choudhary, S. P. Pawar, S. Bose, B. Sahoo, *Phys. Chem. Chem. Phys.* **2017**, *19*, 23268.
- [37] M. Han, X. Yin, K. Hantanasirisakul, X. Li, A. Iqbal, C. B. Hatter, B. Anasori, C. M. Koo, T. Torita, Y. Soda, L. Zhang, L. Cheng, Y. Gogotsi, *Adv. Opt. Mater.* **2019**, *7*, 1900267.
- [38] S. H. Lee, S. Yu, F. Shahzad, W. N. Kim, C. Park, S. M. Hong, C. M. Koo, *Nanoscale* **2017**, *9*, 13432.
- [39] Z. Li, Z. Wang, W. Lu, B. Hou, *Metals* **2018**, *8*, 652.
- [40] R. M. Simon, *Polym.-Plast. Technol. Eng.* **1981**, *17*, 1.
- [41] R. Moore, *Electromagnetic Composites Handbook*, 2nd ed., McGraw-Hill Education, New York **2016**.
- [42] M. Born, E. Wolf, A. B. Bhatia, *Principles of Optics Electromagnetic Theory of Propagation, Interference and Diffraction of Light*, Cambridge University Press, Cambridge **2016**.
- [43] C. C. Katsidis, D. I. Siapkas, *Appl. Opt.* **2002**, *41*, 3978.
- [44] P. He, X.-X. Wang, Y.-Z. Cai, J.-C. Shu, Q.-L. Zhao, J. Yuan, M.-S. Cao, *Nanoscale* **2019**, *11*, 6080.
- [45] X. Li, X. Yin, S. Liang, M. Li, L. Cheng, L. Zhang, *Carbon* **2019**, *146*, 210.
- [46] G. R. Fowles, *Introduction to Modern Optics*, Dover Publications, New York **1989**.
- [47] W. T. Cao, F. F. Chen, Y. J. Zhu, Y. G. Zhang, Y. Y. Jiang, M. G. Ma, F. Chen, *ACS Nano* **2018**, *12*, 4583.
- [48] W. Cao, C. Ma, S. Tan, M. Ma, P. Wan, F. Chen, *Nano-Micro Lett.* **2019**, *11*, 72.
- [49] P. He, M.-S. Cao, Y.-Z. Cai, J.-C. Shu, W.-Q. Cao, J. Yuan, *Carbon* **2020**, *157*, 80.
- [50] F. Xie, F. Jia, L. Zhuo, Z. Lu, L. Si, J. Huang, M. Zhang, Q. Ma, *Nanoscale* **2019**, *11*, 23382.
- [51] L. Wang, L. Chen, P. Song, C. Liang, Y. Lu, H. Qiu, Y. Zhang, J. Kong, J. Gu, *Composites, Part B* **2019**, *171*, 111.
- [52] R. Liu, M. Miao, Y. Li, J. Zhang, S. Cao, X. Feng, *ACS Appl. Mater. Interfaces* **2018**, *10*, 44787.
- [53] Y. Zhang, L. Wang, J. Zhang, P. Song, Z. Xiao, C. Liang, H. Qiu, J. Kong, J. Gu, *Compos. Sci. Technol.* **2019**, *183*, 107833.
- [54] C. Xiang, R. Guo, S. Lin, S. Jiang, J. Lan, C. Wang, C. Cui, H. Xiao, Y. Zhang, *Chem. Eng. J.* **2019**, *360*, 1158.
- [55] K. Raagulan, R. Braveenth, H. J. Jang, Y. Seon Lee, C.-M. Yang, B. Mi Kim, J. J. Moon, K. Y. Chai, *Materials* **2018**, *11*, 1803.
- [56] S.-J. Wang, D.-S. Li, L. Jiang, *Adv. Mater. Interfaces* **2019**, *6*, 1900961.
- [57] L. Liang, G. Han, Y. Li, B. Zhao, B. Zhou, Y. Feng, J. Ma, Y. Wang, R. Zhang, C. Liu, *ACS Appl. Mater. Interfaces* **2019**, *11*, 25399.
- [58] J. W. Jo, J. W. Jung, J. U. Lee, W. H. Jo, *ACS Nano* **2010**, *4*, 5382.
- [59] T. Carey, C. Jones, F. Le Moal, D. Deganello, F. Torrisi, *ACS Appl. Mater. Interfaces* **2018**, *10*, 19948.
- [60] H. S. Sundaram, X. Han, A. K. Nowinski, J.-R. Ella-Menyé, C. Wimbish, P. Marek, K. Senecal, S. Jiang, *ACS Appl. Mater. Interfaces* **2014**, *6*, 6664.
- [61] M. A. Meitl, Y. Zhou, A. Gaur, S. Jeon, M. L. Usrey, M. S. Strano, J. A. Rogers, *Nano Lett.* **2004**, *4*, 1643.
- [62] T. Yun, J.-S. Kim, J. Shim, D. S. Choi, K. E. Lee, S. H. Koo, I. Kim, H. J. Jung, H.-W. Yoo, H.-T. Jung, S. O. Kim, *ACS Appl. Mater. Interfaces* **2017**, *9*, 1021.
- [63] K. Maleski, V. N. Mochalin, Y. Gogotsi, *Chem. Mater.* **2017**, *29*, 1632.
- [64] G.-M. Weng, J. Li, M. Alhabeb, C. Karpovich, H. Wang, J. Lipton, K. Maleski, J. Kong, E. Shaulsky, M. Elimelech, Y. Gogotsi, A. D. Taylor, *Adv. Funct. Mater.* **2018**, *28*, 1803360.
- [65] X. Jin, J. Wang, L. Dai, X. Liu, L. Li, Y. Yang, Y. Cao, W. Wang, H. Wu, S. Guo, *Chem. Eng. J.* **2020**, *380*, 122475.
- [66] L.-X. Liu, W. Chen, H.-B. Zhang, Q.-W. Wang, F. Guan, Z.-Z. Yu, *Adv. Funct. Mater.* **2019**, *29*, 1905197.
- [67] Q.-W. Wang, H.-B. Zhang, J. Liu, S. Zhao, X. Xie, L. Liu, R. Yang, N. Koratkar, Z.-Z. Yu, *Adv. Funct. Mater.* **2019**, *29*, 1806819.
- [68] M. Vural, A. Pena-Francesch, J. Bars-Pomes, H. Jung, H. Gudapat, C. B. Hatter, B. D. Allen, B. Anasori, I. T. Ozbolat, Y. Gogotsi, M. C. Demirel, *Adv. Funct. Mater.* **2018**, *28*, 1801972.
- [69] C. A. Ramírez-Herrera, H. Gonzalez, F. de la Torre, L. Benítez, J. G. Cabañas-Moreno, K. Lozano, *Nanomaterials* **2019**, *9*, 238.
- [70] J. Liu, H. B. Zhang, R. Sun, Y. Liu, Z. Liu, A. Zhou, Z. Z. Yu, *Adv. Mater.* **2017**, *29*, 1702367.
- [71] Z. Fan, D. Wang, Y. Yuan, Y. Wang, Z. Cheng, Y. Liu, Z. Xie, *Chem. Eng. J.* **2020**, *381*, 122696.
- [72] C. Weng, G. Wang, Z. Dai, Y. Pei, L. Liu, Z. Zhang, *Nanoscale* **2019**, *11*, 22804.
- [73] X. Wu, B. Han, H.-B. Zhang, X. Xie, T. Tu, Y. Zhang, Y. Dai, R. Yang, Z.-Z. Yu, *Chem. Eng. J.* **2020**, *381*, 122622.
- [74] L. Wang, H. Qiu, P. Song, Y. Zhang, Y. Lu, C. Liang, J. Kong, L. Chen, J. Gu, *Composites, Part A* **2019**, *123*, 293.
- [75] H. Xu, X. Yin, X. Li, M. Li, S. Liang, L. Zhang, L. Cheng, *ACS Appl. Mater. Interfaces* **2019**, *11*, 10198.
- [76] X.-H. Li, X. Li, K.-N. Liao, P. Min, T. Liu, A. Dasari, Z.-Z. Yu, *ACS Appl. Mater. Interfaces* **2016**, *8*, 33230.
- [77] R. Bian, G. He, W. Zhi, S. Xiang, T. Wang, D. Cai, *J. Mater. Chem. C* **2019**, *7*, 474.
- [78] P. Sambyal, A. Iqbal, J. Hong, H. Kim, M.-K. Kim, S. M. Hong, M. Han, Y. Gogotsi, C. M. Koo, *ACS Appl. Mater. Interfaces* **2019**, *11*, 38046.
- [79] S. Zhao, H. B. Zhang, J. Q. Luo, Q. W. Wang, B. Xu, S. Hong, Z. Z. Yu, *ACS Nano* **2018**, *12*, 11193.
- [80] Z. Zhou, J. Liu, X. Zhang, D. Tian, Z. Zhan, C. Lu, *Adv. Mater. Interfaces* **2019**, *6*, 1802040.
- [81] R. Sun, H. B. Zhang, J. Liu, X. Xie, R. Yang, Y. Li, S. Hong, Z. Z. Yu, *Adv. Funct. Mater.* **2017**, *27*, 1702807.
- [82] J.-Q. Luo, S. Zhao, H.-B. Zhang, Z. Deng, L. Li, Z.-Z. Yu, *Compos. Sci. Technol.* **2019**, *182*, 107754.